UMEÅ UNIVERSITY
Department of Physics
Master's thesis, 30hp

May 9, 2012

Numerical Studies of Vortex Core States in Type II Superconductors

Christin Edblom

c.edblom@mail.nu

Supervisor: Mikael Fogelström, Department of Microtechnology and Nanoscience, Chalmers University of Technology.
Examiner: Andrei Shelankov, Department of Physics, Umeå University

Abstract

In this thesis, we study an isolated vortex in an s-wave superconductor by solving the Bogoliubov-de Gennes equations self-consistently on a disc. We calculate the order parameter and supercurrent profiles, as well as the distribution of quasiparticle states. In contrast to quasi-classical treatments, the ratio Δ_∞/E_F between the order parameter and the Fermi energy is not assumed negligible. We study a regime where this ratio is on the order of 10^{-1}, relevant to high-temperature superconductors. In this regime, we find a Friedel-like oscillation in the order parameter profile at low temperatures. This oscillation is attributed to an increased level spacing of the quasiparticle states, causing a decrease of the number of states present inside the superconducting energy gap. The results are in good agreement with previously published works. In future studies, the method used in this thesis will be generalized to d-wave superconductors.

Sammanfattning

I detta examensarbete studeras en ensam virvel i en s-vågssupraledare genom att självkonsistent lösa Bogoliubov och de Gennes' ekvationer på en cylinderskiva. Vi beräknar ordningsparameter- och superströmsprofiler, samt fördelningen av kvasipartikeltillstånd. Till skillnad från i kvasiklassiska metoder så antas inte kvoten Δ_∞/E_F mellan ordningsparametern och Fermi-energin vara negligerbar. Vi studerar en regim där denna kvot är av storleksordningen 10^{-1}, vilket är fallet i högtemperatur-supraledare. Vid låga temperaturer finner vi i denna regim en Friedelliknande oscillation i ordningsparameterprofilen. Denna oscillations förklaras genom att separationen mellan kvasipartikeltillstånd ökar, vilket får som effekt att färre tillstånd ryms innanför det supraledande energigapet. Våra resultat överensstämmer väl med tidigare publicerade artikler. I framtida studier kommer metoden vi använder i detta examensarbete att generaliseras till d-vågssupraledare.

To Mother

Contents

List of Notations

$\alpha_{j\mu}$	j:th zero of the Bessel function J_μ	16
Δ	Superconducting order parameter	7
Δ_∞	BCS value of the order parameter	3
$\mathcal{E}$	Dimensionless energy, E/T_c	15
$\gamma^\dagger_{n\sigma}$	Quasiparticle creation operator	7
κ	Ginzburg-Landau parameter	5
μ	Angular momentum quantum number	16
ω_c	Cut-off frequency	5
$\psi^\dagger_{k\sigma}$	Field creation operator	6
$\varphi_{j\mu}$	Basis function, normalized Bessel function of the first kind	16
ξ_0	Superconducting coherence length	15
$\xi_k, \xi_{j\mu}$	Normal state energies	9
$c^\dagger_{\mathbf{k}\sigma}$	Electron creation operator	5
c_{nj}, d_{nj}	Series expansion coefficients	16
g_{eff}	Dimesionless coupling constant	19
H_0	Free particle Hamiltonian	6
j_θ	Angular component of supercurrent	29
k_F	Fermi wave number	15
$N(0)$	Density of states at the Fermi surface	12
R	Domain radius	16
T_c	Critical temperature	3
$u_k(\mathbf{r}), v_k(\mathbf{r})$	Full quasiparticle amplitudes	7
$u_{n\mu}(r), v_{n\mu}(r)$	Radial quasiparticle amplitudes	16

List of Figures

1 Introduction

One of today's major unsolved problems in condensed matter physics is to explain the mechanism responsible for high temperature superconductivity, first observed in 1986 [1]. Much effort has been dedicated to determining the symmetry of the superconducting order parameter, since this would narrow the field of possible mechanisms [2]. The cuprates have been shown to have a d-wave symmetry [3, 4].

High-T_c superconductors are type II and thus form vortices. The spectrum of low-energy excitations in a vortex core has been described by Caroli et al. [5]. However, their predictions do not agree with experiments on cuprates [6]. In an attempt to theoretically explain the experimental results, it has been quasi-classically shown [7] that a $d + ip$ vortex state can stabilize in a high-T_c superconductor. However, the angular momentum quantization predicted by Caroli et al. [5] cannot be observed in a quasi-classical regime. This means that in order to quantitatively compare these results to experiments, the same type of states should be found by solving the Bogoliubov-de Gennes (BdG) equations: a fully quantum mechanical procedure. To prepare for such a study, in this thesis we solve the BdG equations in an s-wave superconductor by following Gygi and Schlüter [8]. We calculate the order parameter and supercurrent profiles, and look at the energy and spatial form of some low-lying quasiparticle states. Finally, we study the low-temperature limit of the system, explained in section 3.3.2. In future works, the developed model may be generalized to d- [9] or $d + ip$-states.

The structure of the thesis is as follows. Chapter 2 deals with the theoretical background and introduces all the terminology needed to understand the above paragraphs. We start with a short review of concepts and superconducting phenomena relevant to this thesis. A proper discussion of the basics of superconductivity can be found in the literature, for example in Tinkham [10]. We continue with a detailed derivation of the BdG equations from the BCS theory in section 2.2, and the gap equation is derived and explained. Finally, we take a closer look at quasiparticles and investigate flux quantization. Chapter 3 details the mathematics involved in translating the BdG equations into a numerical model, and replicates some known results of s-wave superconductors.

The reader is assumed to be familiar with basic solid state physics to the level of Ashcroft and Mermin [11]. To understand the background and some of the calculations it is helpful to have some knowledge of mean field methods and second quantization. We use units in which $\hbar = k_B = 1$; temperature, frequency and energy thus have the same dimensionality.

2 Superconductivity: an overview

Here, we give the necessary theoretical background. We begin with a very brief review of superconductivity, primarily intended to introduce terminology and concepts. The focus here is on properties of superconductors when a magnetic field is applied. A derivation of the BdG equations and the gap equation follows, and flux quantization is discussed.

2.1 Basic concepts

A superconductor is a material that, below a certain temperature (the critical temperature T_c), displays a vanishingly small electrical resistance. Such a material was first observed in 1911 by the Dutch physicist Kamerlingh Onnes [12], when he measured the resistance of a solid mercury wire cooled below 4.2 K.

This phenomenon was not understood until the late 1950's, when the Bardeen-Cooper-Schreiffer (BCS) theory [13] explained superconductivity through the formation of Cooper pairs. At or below the critical temperature, electrons near the Fermi surface are coupled together into pairs by the lattice vibrations [14]. In other words, the electron-electron interaction is phonon-mediated. This boson-like state is called a BCS-condensate and is similar to the superfluid state of an interacting boson gas; a connection which is explored by Bogoliubov et al. [15].

One central result in the BCS theory is that, as a material transitions into the superconducting state, a temperature-dependent energy gap $2\Delta_\infty(T)$ opens up. Furthermore, for weak interaction superconductivity BCS showed that $\Delta_\infty(0) = 1.76\ T_c$; a quantitative result in good agreement with experimental data for many different materials.

Before the BCS theory, Landau and Ginzburg argued [16] that the free energy of a superconductor can be expressed as a function of a complex pseudo-wave function ψ, related to the density of superconducting electrons as $|\psi|^2 = n_s$. The energy gap is allowed to vary spatially and plays the role of an order parameter [10], proportional to n_s. Gor'kov [17] has shown that the two descriptions of superconductivity are consistent with each other.

The azimuthal quantum number l [18] of the Cooper pair names the "wave" character of the superconductor [19]; an s-wave superconductor has $l = 0$, etc. The spin quantum number S also comes into play; s- and d-wave are spin singlet states while the p-wave is a spin triplet. We recall that since we deal with fermions, the two-particle wave function of a Cooper pair has to be anti-symmetric. There is then only one possibility for $S = 0$: the state $2^{-1/2}\big(|\uparrow\downarrow\rangle - |\downarrow\uparrow\rangle\big)$. This is the spin singlet. In contrast, for $S = 1$ we have the

three possibilities $|\uparrow\uparrow\rangle$, $2^{-1/2}\big(|\uparrow\downarrow\rangle + |\downarrow\uparrow\rangle\big)$ and $|\downarrow\downarrow\rangle$ with z-projections $S_z = 1, 0$ and -1 respectively. Application of a magnetic field lifts the degeneracy of the triplet; we may think of a p-wave superconductor as having magnetic Cooper pairs.

Historically, it was believed that T_c could be no higher than ≈ 30 K. Superconductors whose critical temperature does in fact exceed this are called high-T_c. In such, Cooper pair formation has to be mediated by some other mechanism than phonons. Exactly how this mechanism looks is an active field of research. One possibility is that the electrons are coupled together by spin fluctuations [20]. These can be anti-ferromagnetic, leading to a d-wave order parameter, or ferromagnetic, leading to a p-wave order parameter [2].

High-T_c materials include iron-based superconductors with critical temperatures around $40 - 50$ K [21] as well as copper-oxide based materials (cuprates). Because of their early emergence and high critical temperature – above the boiling point of nitrogen at atmospheric pressure – much research has been devoted to cuprates. They have been shown [3, 4] to have predominantly $d_{x^2-y^2}$-symmetry, possibly with s- or p-wave components mixed in.

2.1.1 Applied magnetic field

Below the critical temperature, superconductivity can be destroyed by the application of an external magnetic field. This phase transition from the superconducting state to the normal state can be either of first or second order. This gives rise to two types of superconductors, referred to as type I and type II corresponding to the order of the phase transition. Most pure metals are type I; all high-T_c superconductors are type II.

A property of type I materials is the Meissner effect [11]; if the superconductor is placed in a magnetic field smaller than the material-specific critical field $H_c(T)$ it acts as a near-perfect diamagnet. The magnetic flux inside the superconductor decreases as $e^{-r/\lambda}$ where r is radial distance measured from the edge of the solid and λ is called the penetration depth. If the magnetic field is increased past $H_c(T)$, the superconductor transitions into the normal state.

In type II superconductors, the Meissner effect is incomplete and magnetic flux does penetrate, as investigated by Abrikosov [22]. When a magnetic field below the lower critical field $H_{c1}(T)$ is applied on a type II superconductor, it acts like a type I material and expels all magnetic flux. If the field in increased past $H_{c1}(T)$, a mixed state is formed. In this state, normal regions which admit magnetic flux are surrounded by superconducting regions. As the magnetic field is increased, the fraction of volume occupied by normal regions increases. When the upper critical field $H_{c2}(T)$ is reached, superconductivity is destroyed. As shown in section 2.2.4, the requirement that the order parameter is single valued leads to flux quantization; the normal regions in a type II superconductor only admit certain values of magnetic flux.

One can show [16] that the surface energy of an interface between the superconducting and the normal state of a material is positive for type I materials and negative for type II. In other words, in a type II superconductor it is ener-

getically preferable to form normal domains which admit magnetic flux, rather than to expel all magnetic flux. Away from the interface, the superconducting phase has a lower energy than the normal phase. It follows that the domains that minimize energy are those with the greatest surface to volume ratio, such as long, thin cylinders. In analogy with the superfluid case these filaments are called vortex lines, and form a regular lattice. A triangular lattice has the lowest energy, but the symmetry can be altered by inhomogeneities in the material.

The Ginzburg-Landau (GL) theory introduced an additional characteristic length scale: the coherence length ξ. Qualitatively, we may view λ as the length scale over which the magnetic field in the solid changes appreciably and ξ as the length scale over which the order parameter changes. Both λ and ξ depend on temperature in the same way; the temperature-independent ratio $\kappa = \lambda/\xi$ is called the Ginzburg-Landau parameter. Superconductors where $\kappa > 1/\sqrt{2}$ are type II [22], and those with $\kappa < 1/\sqrt{2}$ are type I.

2.2 From BCS to BdG

The BCS theory is not ideally suited for a treatment of type II superconductors with vortices present. Instead, we will use the Bogoliubov-de Gennes (BdG) equations, a superconducting analogue of the Schrödinger equation. This derivation of the BdG equations follows de Gennes [23]. Here, we deal with s-wave superconductors; for other pairing symmetries the coupling "constant" g carries a $\mathbf{k}$-dependence.

In pure materials, the wave vector $\mathbf{k}$ is a good quantum number. In the BCS one thus uses the pairing Hamiltonian

$$H_{BCS} = \sum_{\mathbf{k}\sigma} c^\dagger_{\mathbf{k}\sigma} H_0' c_{\mathbf{k}\sigma} - g \sum_{\mathbf{k},\mathbf{l}} c^\dagger_{\mathbf{k}\uparrow} c^\dagger_{-\mathbf{k}\downarrow} c_{-\mathbf{l}\downarrow} c_{\mathbf{l}\uparrow} \tag{2.1}$$

Here $c^\dagger_{\mathbf{k}\sigma}$ ($c_{\mathbf{k}\sigma}$) are creation (annihilation) operators for electrons with momentum $\mathbf{k}$ and spin σ. In all sums over $\mathbf{k}$ there is a cut-off implied to prevent divergence; we sum only over states such that the energy $|E_{\mathbf{k}}| < \omega_c$. BCS chose this cut-off to be the Debye frequency; since the Cooper pair formation is phonon mediated this is physically motivated. As we shall see in section 3.1.1, our results do not depend on the exact value of the cut-off frequency, so we will not specify it further.

We see that the pair interaction term with coupling constant $g > 0$ scatters a pair of electrons from the state $|\mathbf{l}\uparrow, -\mathbf{l}\downarrow\rangle$ to the state $|\mathbf{k}\uparrow, -\mathbf{k}\downarrow\rangle$. H_0' is the one-particle Hamiltonian

$$H_0' = \frac{1}{2m}\left(-i\nabla - \frac{e}{c}\mathbf{A}(\mathbf{r})\right)^2 - E_F \tag{2.2}$$

with magnetic vector potential $\mathbf{A}(\mathbf{r})$. Note that the subtraction of the Fermi energy E_F means that the eigenvalues of this operator are energies measured relative to E_F.

2.2.1 The Bogoliubov transformation

In a material with impurities or other spatial inhomogeneities, $\mathbf{k}$ is not a good quantum number and we must find another way to model the situation. To include such effects, we add an external potential $U(\mathbf{r})$ to the one-particle Hamiltonian:

$$H_0 = \frac{1}{2m}\left(-i\nabla - \frac{e}{c}\mathbf{A}\right)^2 + U(\mathbf{r}) - E_F. \tag{2.3}$$

Next, we form position-dependent field creation and annihilation operators:

$$\begin{aligned}\psi_\sigma^\dagger(\mathbf{r}) &= \sum_{\mathbf{k}} \zeta_{\mathbf{k}}^*(\mathbf{r}) c_{\mathbf{k}\sigma}^\dagger, \\ \psi_\sigma(\mathbf{r}) &= \sum_{\mathbf{k}} \zeta_{\mathbf{k}}(\mathbf{r}) c_{\mathbf{k}\sigma}.\end{aligned} \tag{2.4}$$

The field operators creates (annihilates) a particle at position $\mathbf{r}$, which has momentum $\mathbf{k}$ with probability $|\zeta_{\mathbf{k}}|^2$. As always, we may view the annihilation of electrons as creation of holes instead.

De Gennes [23] uses exponential functions $e^{i\mathbf{k}\cdot\mathbf{r}}$ for the coefficients $\zeta_{\mathbf{k}}(\mathbf{r})$, but any complete, orthonormal set of functions will do, with the added condition that $\zeta_{-\mathbf{k}}^*(\mathbf{r}) = \zeta_{\mathbf{k}}(\mathbf{r})$. This is because of that annihilating a particle with momentum $\mathbf{k}$ has the same effect on the total momentum of the field as creating a particle with momentum $-\mathbf{k}$.

Using $\zeta_{\mathbf{k}}(\mathbf{r}) = \langle \mathbf{r} \,|\, \zeta_{\mathbf{k}} \rangle$ and the resolution of identity $\mathbb{1} = \sum_{\mathbf{k}} |\zeta_{\mathbf{k}}\rangle \langle \zeta_{\mathbf{k}}|$, it is straight-forward to show that the field operators satisfy the regular fermion commutation relations. That is,

$$\left[\psi_\sigma^\dagger(\mathbf{r}), \psi_\tau(\mathbf{r}')\right]_+ = \delta_{\sigma\tau}\ \delta(\mathbf{r} - \mathbf{r}') \tag{2.5}$$

and all other anticommutators zero. Here, δ is used both for the Kronecker delta and Dirac's delta-function; the ambiguity is cleared up by the indicies or arguments.

We wish to invert the relations (2.4) to enable direct substitution into equation (2.1). To accomplish this, multiply $\psi_\sigma(\mathbf{r})$ with $\zeta_{\mathbf{k}}^*(\mathbf{r}) = \langle \zeta_{\mathbf{k}} \,|\, \mathbf{r} \rangle$ and integrate over $\mathbf{r}$:

$$\begin{aligned}\int \mathrm{d}\mathbf{r}\ \zeta_{\mathbf{k}}^*(\mathbf{r})\psi_\sigma(\mathbf{r}) &= \sum_{\mathbf{k}'} \int \mathrm{d}\mathbf{r}\ \ \langle \zeta_{\mathbf{k}} \,|\, \mathbf{r} \rangle \langle \mathbf{r} \,|\, \zeta_{\mathbf{k}'} \rangle\, c_{\mathbf{k}'\sigma} \\ &= \sum_{\mathbf{k}'} \langle \zeta_{\mathbf{k}} \,|\, \zeta_{\mathbf{k}'} \rangle\, c_{\mathbf{k}'\sigma} = c_{\mathbf{k}\sigma}\end{aligned} \tag{2.6}$$

since $\mathbb{1} = \int \mathrm{d}\mathbf{r}\ \ |\mathbf{r}\rangle \langle \mathbf{r}|$ and $\langle \zeta_{\mathbf{k}} \,|\, \zeta_{\mathbf{k}'} \rangle = \delta_{\mathbf{k}\mathbf{k}'}$. Analogously, we find that

$$c_{\mathbf{k}\sigma}^\dagger = \int \mathrm{d}\mathbf{r}\ \zeta_{\mathbf{k}}(\mathbf{r})\psi_\sigma^\dagger(\mathbf{r}). \tag{2.7}$$

Before substituting we simplify the interaction term

$$-g \sum_{\mathbf{k},\mathbf{l}} c_{\mathbf{k}\uparrow}^\dagger c_{-\mathbf{k}\downarrow}^\dagger c_{-\mathbf{l}\downarrow} c_{\mathbf{l}\uparrow} \tag{2.8}$$

by a mean field assumption. Instead of scattering a Cooper pair labeled by $\mathbf{l}$ into that labeled by $\mathbf{k}$, we simply destroy the $\mathbf{l}$-pair and create the $\mathbf{k}$-pair, averaging out the interaction. The sum (2.8) becomes

$$-g\sum_{\mathbf{k},\mathbf{l}}\left[\langle c^\dagger_{\mathbf{k}\uparrow}c^\dagger_{-\mathbf{k}\downarrow}\rangle c_{-\mathbf{l}\downarrow}c_{\mathbf{l}\uparrow}+c^\dagger_{\mathbf{k}\uparrow}c^\dagger_{-\mathbf{k}\downarrow}\langle c_{-\mathbf{l}\downarrow}c_{\mathbf{l}\uparrow}\rangle\right]. \tag{2.9}$$

Since there is no longer any interaction between the annihilated and the created pair, particle number is not necessarily conserved. We think of the pairs as coming from or joining a many-particle condensate acting as a reservoir.

We note that $\langle c^\dagger_{\mathbf{k}\uparrow}c^\dagger_{-\mathbf{k}\downarrow}\rangle = \langle c_{-\mathbf{k}\downarrow}c_{\mathbf{k}\uparrow}\rangle^*$, and define

$$\Delta(\mathbf{r}) = -g\sum_{\mathbf{l}}\langle c_{-\mathbf{l}\downarrow}c_{\mathbf{l}\uparrow}\rangle = -g\langle\psi_\downarrow(\mathbf{r})\psi_\uparrow(\mathbf{r})\rangle = g\langle\psi_\uparrow(\mathbf{r})\psi_\downarrow(\mathbf{r})\rangle. \tag{2.10}$$

Relabeling the summation indicies $\mathbf{k}\to\mathbf{l}$ and $\mathbf{l}\to\mathbf{k}$ in the first term of (2.9), we find

$$\sum_{\mathbf{k}}\left[\Delta^*(\mathbf{r})c_{-\mathbf{k}\downarrow}c_{\mathbf{k}\uparrow}+\Delta(\mathbf{r})c^\dagger_{\mathbf{k}\uparrow}c^\dagger_{-\mathbf{k}\downarrow}\right]. \tag{2.11}$$

Substituting equation (2.4) in equation (2.1) with the second sum replaced by (2.11), we arrive at the effective Hamiltonian

$$H_{\mathit{eff}} = \int \mathrm{d}\mathbf{r}\ \left[\psi^\dagger_\sigma H_0\psi_\sigma+\Delta\psi^\dagger_\uparrow\psi^\dagger_\downarrow+\Delta^*\psi_\uparrow\psi_\downarrow\right]. \tag{2.12}$$

Summation over repeated spin indicies σ is implied and the $\mathbf{r}$-dependence of the operators has been suppressed for readability. This is a quadratic form in ψ_σ and $\psi^\dagger_\sigma$, and it is a result of elementary linear algebra that any quadratic form can be diagonalized by performing a unitary transformation [24].

To this end, we write

$$\begin{aligned}\psi_\uparrow(\mathbf{r}) &= \sum_n\left(\gamma_{n\uparrow}u_n(\mathbf{r})-\gamma^\dagger_{n\downarrow}v^*_n(\mathbf{r})\right),\\ \psi_\downarrow(\mathbf{r}) &= \sum_n\left(\gamma_{n\downarrow}u_n(\mathbf{r})+\gamma^\dagger_{n\uparrow}v^*_n(\mathbf{r})\right).\end{aligned} \tag{2.13}$$

$\gamma^\dagger_{n\sigma}$ and $\gamma_{n\sigma}$ are creation and annihilation operators for excitations in the superconductor, which we call quasiparticles. We shall return to these in section 2.2.2.

We demand that $\gamma_{n\sigma},\gamma^\dagger_{n\sigma}$ satisfy fermionic commutation relations:

$$\left[\gamma^\dagger_{m\tau},\gamma_{n\sigma}\right]_+ = \delta_{mn}\delta_{\sigma\tau},\quad \left[\gamma_{n\sigma},\gamma_{m\tau}\right]_+ = \left[\gamma^\dagger_{n\sigma},\gamma^\dagger_{m\tau}\right]_+ = 0. \tag{2.14}$$

We require that equation (2.13) diagonalizes the Hamiltonian, that is,

$$H_{\mathit{eff}} = E_G+\sum_{n\sigma}E_n\gamma^\dagger_{n\sigma}\gamma_{n\sigma} \tag{2.15}$$

where E_G is the ground state energy and E_n the energy of the n:th excitation. It is possible to obtain this result by brute force: substitute (2.13) in (2.12),

simplify the expression using the commutations relations (2.14) and fix u_n and v_n by requiring that the coefficients of any off-diagonal terms are zero. This is extremely tedious, and a more elegant solution is the following.

We use equation (2.13) and (2.15) to calculate the commutators

$$\begin{aligned}[H_{\mathit{eff}}, \gamma_{n\sigma}] &= -E_n \gamma_{n\sigma}, \\ \left[H_{\mathit{eff}}, \gamma^\dagger_{n\sigma}\right] &= E_n \gamma^\dagger_{n\sigma}. \end{aligned} \tag{2.16}$$

If we instead use H_{eff} in the form (2.12) and the anticommutation properties of ψ_σ, we can calculate

$$\begin{aligned}[\psi_\uparrow(\mathbf{r}), H_{\mathit{eff}}] &= \int \mathrm{d}\mathbf{r}\,' \Big(\left[\psi_\uparrow(\mathbf{r}), \psi^\dagger_\sigma(\mathbf{r}') H_0 \psi_\sigma(\mathbf{r}')\right] + \\ &\qquad [\psi_\uparrow(\mathbf{r}), \Delta(\mathbf{r}')\psi^\dagger_\uparrow(\mathbf{r}')\psi^\dagger_\downarrow(\mathbf{r}')] + [\psi_\uparrow(\mathbf{r}), \Delta^*(\mathbf{r}')\psi_\uparrow(\mathbf{r}')\psi_\downarrow(\mathbf{r}')] \Big) \\ &= \int \mathrm{d}\mathbf{r}\,' \Big(\delta(\mathbf{r}-\mathbf{r}') H_0 \psi_\uparrow(\mathbf{r}') + \Delta(\mathbf{r}')\delta(\mathbf{r}-\mathbf{r}')\psi^\dagger_\downarrow(\mathbf{r}') + 0 \Big) \\ &= H_0\psi_\uparrow(\mathbf{r}) + \Delta(\mathbf{r})\psi^\dagger_\downarrow(\mathbf{r}). \end{aligned} \tag{2.17}$$

Analogously, we find that

$$[\psi_\downarrow(\mathbf{r}), H_{\mathit{eff}}] = H_0\psi_\downarrow(\mathbf{r}) - \Delta(\mathbf{r})\psi^\dagger_\uparrow(\mathbf{r}). \tag{2.18}$$

Now we wish to substitute equation (2.13) on both sides of equations (2.17) and (2.18). However, both equations turn out to give the same end result, so if suffices to deal with one of them.

With the help of equation (2.16), the left hand side of equation (2.17) becomes

$$\begin{aligned}[\psi_\uparrow(\mathbf{r}), H_{\mathit{eff}}] &= \sum_n \Big(\left[\gamma_{n\uparrow}, H_{\mathit{eff}}\right] u_n(\mathbf{r}) - [\gamma^\dagger_{n\downarrow}, H_{\mathit{eff}}] v^*_n(\mathbf{r}) \Big) \\ &= \sum_n \Big(E_n u_n(\mathbf{r})\gamma_{n\uparrow} + E_n v^*_n(\mathbf{r})\gamma^\dagger_{n\downarrow} \Big) \end{aligned} \tag{2.19}$$

and the right hand side is

$$H_0\psi_\uparrow(\mathbf{r}) + \Delta(\mathbf{r})\psi^\dagger_\downarrow(\mathbf{r}) = \sum_n \Big((H_0 u_n + \Delta v_n)\gamma_{n\uparrow} + (-H_0 v^*_n + \Delta u^*_n)\gamma^\dagger_{n\downarrow} \Big). \tag{2.20}$$

Equating the coefficients of $\gamma_{n\uparrow}$ and $\gamma^\dagger_{n\downarrow}$ in equations (2.19) and (2.20), we find that we have derived the Bogoliubov-de Gennes equations:

$$\begin{aligned} H_0 u_n(\mathbf{r}) + \Delta(\mathbf{r}) v_n(\mathbf{r}) &= E_n u_n(\mathbf{r}) \\ -H_0 v_n(\mathbf{r}) + \Delta^*(\mathbf{r}) u_n(\mathbf{r}) &= E_n v_n(\mathbf{r}) \end{aligned} \tag{2.21}$$

where we have conjugated both sides of the second equation, using that H_0 is Hermitian.

It is instructive to rewrite equation (2.21) in matrix form:

$$\begin{pmatrix} H_0 & \Delta \\ \Delta^* & -H_0 \end{pmatrix} \begin{pmatrix} u_n \\ v_n \end{pmatrix} = E_n \begin{pmatrix} u_n \\ v_n \end{pmatrix}. \tag{2.22}$$

We see that the coefficient matrix is Hermitian; it follows that the different eigenvectors (u_n, v_n) can be chosen to be orthonormal [24].

2.2.2 Quasiparticles

We will now look closer at the quantities $u_n(\mathbf{r})$ and $v_n(\mathbf{r})$; it is high time to consider what these abstract quasiparticles actually are.

From equation (2.13), we form the quantity

$$\int \mathrm{d}\mathbf{r} \left(u_n^* \psi_\uparrow + v_n^* \psi_\downarrow^\dagger \right) = \sum_m \int \mathrm{d}\mathbf{r} \left((u_n^* u_m + v_n^* v_m)\, \gamma_{m\uparrow} + (v_n^* u_m^* - u_n^* v_m^*)\, \gamma_{m\downarrow}^\dagger \right), \tag{2.23}$$

and using the orthogonality relations [25]

$$\begin{aligned} \int \mathrm{d}\mathbf{r}\, (u_n^* u_m + v_n^* v_m) &= \delta_{mn} \\ \int \mathrm{d}\mathbf{r}\, (v_n^* u_m^* - u_n^* v_m^*) &= 0 \end{aligned} \tag{2.24}$$

we find the inverted definition

$$\gamma_{n\uparrow} = \int \mathrm{d}\mathbf{r} \left(u_n^* \psi_\uparrow + v_n^* \psi_\downarrow^\dagger \right). \tag{2.25}$$

Similarily

$$\gamma_{n\downarrow} = \int \mathrm{d}\mathbf{r} \left(u_n^* \psi_\downarrow - v_n^* \psi_\uparrow^\dagger \right). \tag{2.26}$$

Remembering the definition (2.4) of the field operators, we now see that the quasiparticles created by $\gamma_{n\sigma}^\dagger$ are superpositions of $c_{\mathbf{k}\sigma}^\dagger$ and $c_{\mathbf{k}\sigma}$. That is, the quasiparticles are superpositions of electron and hole states. The amplitude u_n (v_n) indicate the probability of an excitation being in an electron-like (hole-like) state.

We will now derive explicit expressions for the quasiparticle amplitudes and the excitation energies E_n. We use equation (2.22), and assume zero magnetic field. The operator H_0 is replaced with its eigenvalue ξ_n: by setting $\Delta = 0$ we see that ξ_n is the energy of the n:th excitation in the normal state. The eigenvalue problem (2.22) then has the characteristic equation

$$0 = \begin{vmatrix} \xi_n - E_n & \Delta \\ \Delta^* & -\xi_n - E_n \end{vmatrix} = -\xi_n^2 + E_n^2 - |\Delta|^2, \tag{2.27}$$

so the eigenvalues are – neglecting the negative root – $E_n = \sqrt{\xi_n^2 + |\Delta|^2}$. We recall that in the BCS theory, Δ is constant: it immediately follows that $E_{min} = |\Delta|$ as expected.

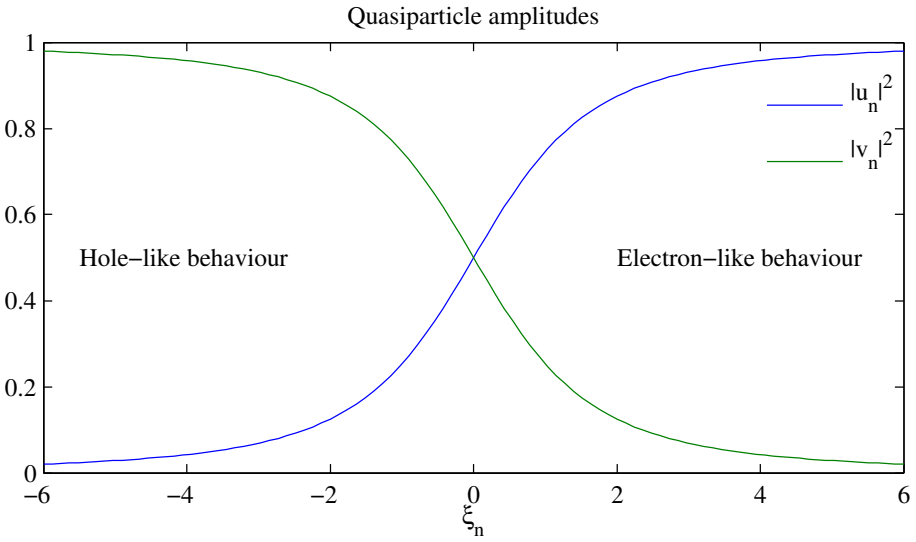

Figure 2.1: Plot of the amplitudes determined in equation (2.30), illustrating the different regimes of hole-like and electron-like behaviour.

To find the eigenvectors, we look at the second row in equation (2.21):

$$-\xi_n v_n + \Delta^* u_n = E_n v_n, \tag{2.28}$$

or

$$v_n = \frac{\Delta^*}{\xi_n + E_n} u_n. \tag{2.29}$$

We multiply each side with its complex conjugate, replace $|v_n|^2$ with $1 - |u_n|^2$ (since the eigenvector (u_n, v_n) was normalized) on the left hand side and solve for $|u_n|^2$. In the end, we find

$$|u_n|^2 = \frac{1}{2}\left(1 + \frac{\xi_n}{E_n}\right) \qquad \text{so} \qquad |v_n|^2 = \frac{1}{2}\left(1 - \frac{\xi_n}{E_n}\right), \tag{2.30}$$

as plotted in figure. 2.1.

We note that $E_n = \sqrt{\xi_n^2 + |\Delta|^2} \to |\xi_n|$ when $|\xi_n| \gg |\Delta|$. From equation (2.30) we then see that, as ξ_n increases from $-\infty$ through zero and to $+\infty$, the corresponding quasiparticle changes from behaving completely like an electron, to being an equal mixture of an electron and a hole, to behaving completely like a hole. This means that interactions that change the value of ξ, like scattering processes, will alter the physical characteristics of the quasiparticle.

Looking again at equation (2.21), by direct substitution we can show that if (u_n, v_n) is the eigenvector corresponding to the eigenvalue E_n, $(-v_n^*, u_n^*)$ is the eigenvector corresponding to $-E_n$. In light of the above discussion, we see that this transformation means that for every quasiparticle with energy E_n in an excited state above the Fermi surface, there is one with the opposite electron-hole characteristic and energy $-E_n$ below the Fermi surface. For the extreme cases where either u_n or v_n are close to zero, this is completely analogous to

the particle-hole symmetry in a normal metal. We may view the paired $\pm E_n$-solutions as "positive" and "negative" quasiparticle excitations. For this reason, we only consider the positive E_n from here on - we only look at the excitations above the Fermi surface and obtain those below with a simple transformation.

2.2.3 The gap equation

From the definition (2.10) we may now explicitly calculate Δ. We will use the mean value rules [23]

$$\langle \gamma_{n\sigma}\gamma_{m\tau}\rangle = 0 \qquad \text{and} \qquad \left\langle \gamma^\dagger_{n\sigma}\gamma_{m\tau}\right\rangle = \delta_{nm}\delta_{\sigma\tau}f(E_n), \tag{2.31}$$

where

$$f(E_n) = \frac{1}{1+e^{E_n/T}} \tag{2.32}$$

is the Fermi distribution. Substituting (2.13) in (2.10), we get

$$\begin{aligned}
\Delta &= g\left\langle \sum_{m,n}\left(\gamma_{n\uparrow}u_n - \gamma^\dagger_{n\downarrow}v^*_n\right)\left(\gamma_{m\downarrow}u_m + \gamma^\dagger_{m\uparrow}v^*_m\right)\right\rangle \\
&= g\sum_{m,n}\left(\left\langle \gamma_{n\uparrow}\gamma^\dagger_{m\uparrow}\right\rangle v^*_m u_n - \left\langle \gamma^\dagger_{n\downarrow}\gamma_{m\downarrow}\right\rangle v^*_n u_m\right) \\
&= g\sum_{m,n}\left(v^*_n u_m\delta_{mn}(1-f(E_n)) - v^*_m u_n\delta_{mn}f(E_m)\right) \\
&= g\sum_n v^*_n u_n(1-2f(E_n)) \\
&= g\sum_n v^*_n u_n \tanh\left(\frac{E_n}{2T}\right).
\end{aligned} \tag{2.33}$$

The factor $\tanh(E_n/2T)$ is real, so we must have that the phase of Δ is equal to the phase of $v^*_n u_n$. If the u_n are chosen real and positive, from equation (2.30) we find

$$u_n = \frac{1}{\sqrt{2}}\left(1+\frac{\xi_n}{E_n}\right)^{1/2}, \qquad v_n = \frac{1}{\sqrt{2}}\left(1-\frac{\xi_n}{E_n}\right)^{1/2} e^{i\phi} \tag{2.34}$$

and $\Delta = |\Delta|e^{-i\phi}$. Then, $v^*_n u_n = \Delta/2E_n$. This result is general, and is valid even if u_n is not chosen real. We thus arrive at the self-consistency equation for the energy gap:

$$\Delta = g\sum_n \frac{\Delta}{2\sqrt{\xi_n^2+|\Delta|^2}}\tanh\left(\frac{\sqrt{\xi_n^2+|\Delta|^2}}{2T}\right), \tag{2.35}$$

or

$$1 = g\sum_n \frac{1}{2\sqrt{\xi_n^2+|\Delta|^2}}\tanh\left(\frac{\sqrt{\xi_n^2+|\Delta|^2}}{2T}\right). \tag{2.36}$$

This is the gap equation, to be solved self-consistently for Δ. In practise we do this by relaxation; we guess a value of Δ, insert on the right side of equation (2.35) and calculate a new value. This process is repeated until $\Delta_{old} = \Delta_{new}$.

The coupling constant g can be determined as follows: at $T = T_c$, $\Delta = 0$ and $E_n = \xi_n$. We transform the sum in equation (2.36) into an integral, and find

$$\begin{aligned}\frac{1}{g} &= \int_{-\omega_c}^{\omega_c} \mathrm{d}\xi \; N(\xi) \frac{1}{2|\xi|} \tanh\left(\frac{|\xi|}{2T_c}\right). \\ &= N(0) \int_0^{\omega_c} \mathrm{d}\xi \; \frac{1}{\xi} \tanh\left(\frac{\xi}{2T_c}\right). \end{aligned} \tag{2.37}$$

We have assumed that the density of states $N(\xi)$ is slowly varying over the integration interval, and thus factored out the constant $N(0)$ – the density of states at the Fermi surface. This integral can be solved exactly [10], and yields

$$\frac{1}{g} = N(0) \ln\left(\frac{2e^{\gamma}\omega_c}{\pi T_c}\right) \approx N(0) \ln\left(1.13\omega_c/T_c\right) \tag{2.38}$$

where γ is Euler's constant, the three first digits of which are 0.577.

2.2.4 Flux quantization

One rather counter-intuitive phenomenon is the quantization of magnetic flux inside normal regions surrounded by superconducting regions – which is exactly what a vortex is. The existence of this phenomenon has been experimentally verified since the 1960's [26, 27].

We can understand this by looking at the definition of the magnetic flux through a surface S:

$$\Phi = \iint_S \mathrm{d}\mathbf{S} \; \cdot \mathbf{B} \tag{2.39}$$

where $\mathbf{B}$ is the magnetic field. Using the definition $\mathbf{B} = \nabla \times \mathbf{A}$ and Stokes' theorem, we may write the magnetic flux as

$$\Phi = \oint_C \mathrm{d}\ell \cdot \mathbf{A}, \tag{2.40}$$

where the contour C is the boundary of S.

As is well known [28], the magnetic potential $\mathbf{A}$ is not unique: any gauge transformation of the form

$$\mathbf{A}' = \mathbf{A} + \nabla\chi \tag{2.41}$$

leaves the magentic field unchanged. One can show [23] that the eigenvalues of the BdG equations (2.21) – and indeed all measurable quantities – are unchanged by such a transformation, but the quasiparticles wave functions and the pair potential are not. When replacing $\mathbf{A}$ with $\mathbf{A}'$, the new pair potential is

$$\Delta'(\mathbf{r}) = \Delta(\mathbf{r}) e^{i2e\chi/\hbar c}. \tag{2.42}$$

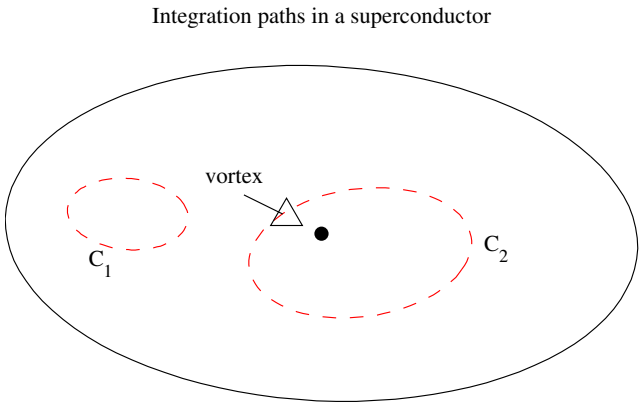

Figure 2.2: The curve C_1 shows a path in a region where $\mathbf{B} = 0$. C_2 encircles the vortex but is far enough away from it so that $\mathbf{B} = 0$ on C_2.

In this section, we reintroduce $\hbar$ for clarity.

Physically, $\Delta(\mathbf{r}) = |\Delta(\mathbf{r})|e^{i\phi(\mathbf{r})}$ must be single valued. This means that, for any closed contour C,

$$\oint_C \mathrm{d}\ell \cdot \nabla\phi = 2\pi m, \ m \in \mathbb{Z}. \tag{2.43}$$

That is, the change in ϕ as we move around C must be an integer multiple of 2π. The gauge transformation (2.42) can also be written as $\phi \to \phi + 2e\chi/\hbar c$; it follows that

$$\frac{2e}{\hbar c}\oint_C \mathrm{d}\ell \cdot \nabla\chi = 2\pi n, \ n \in \mathbb{Z}. \tag{2.44}$$

Now, assume we place the surface S (in figure 2.2, $\partial S = C_1$) deep inside a superconductor where $\mathbf{B} = 0$; by equation (2.39) then so is the magnetic flux through S. If we instead choose S such that it is penetrated by a vortex line (in figure 2.2, $\partial S = C_2$) , the magnetic field will not be zero in all of S and the flux is non-zero. We may, however, place the boundary C deep enough in the superconductor so that $\mathbf{B} = 0$ on C. It is then permissible to write the vector potential $\mathbf{A} = \nabla\chi$, and

$$\Phi = \oint_C \mathrm{d}\ell \cdot \mathbf{A} = \oint_C \mathrm{d}\ell \cdot \nabla\chi = \frac{\hbar c}{2e} 2\pi n = \Phi_0 n. \tag{2.45}$$

In the last step we define the quantum of flux:

$$\Phi_0 = \frac{2\pi\hbar c}{2e} = \frac{hc}{2e}. \tag{2.46}$$

In real situations, each vortex almost always contains only one flux quantum.

With the theoretical background thus established, we now move on to the actual solution of the Bogoliubov-de Gennes equation (2.21).

3 The quasiparticle core states

In this chapter, we develop a numerical method for the solution of the BdG equations near a vortex line. We work in the extreme type II-limit, in which $\kappa = \lambda/\xi \gg 1$. As mentioned in section 2.1.1, the penetration depth λ is the characteristic length scale for the magnetic field, and ξ is the characteristic length scale for the order parameter. So if $\lambda \gg \xi$, the magnetic field will vary very slowly compared to the order parameter. When looking at how the order parameter changes, the magnetic field will then be a near-constant background which we can ignore. In practise we drop $\mathbf{A}(\mathbf{r})$ from the BdG equations.

For this system, it is natural to work in cylindrical coordinates. We will model a pure cylindrical superconductor with radius R and a single, isolated vortex situated at $r = 0$. As we shall see it will suffice to solve for the r-dependence of the order parameter and quasiparticle wave functions. The effect of the external potential $U(\mathbf{r})$ is included by shifting to an effective mass m^*.

3.1 Setting up the problem

To solve the BdG-equations numerically, we first wish to write them in a dimensionless form. The characteristic parameters will be the zero-temperature value of the superconducting coherence length: $\xi_0 = v_F/\Delta_\infty(0)$, used as the unit of distance, and the critical temperature T_c, used as the unit of energy. We define

$$\mathbf{x} = \frac{\mathbf{r}}{\xi_0}, \qquad \nabla^2_{\mathbf{x}} = \xi_0^2 \nabla^2_{\mathbf{r}} \qquad \text{and} \qquad \mathcal{E} = \frac{E}{T_c}. \tag{3.1}$$

Using that

$$T_c \simeq \Delta_\infty(0) = \frac{v_F}{\xi_0} = \frac{k_F}{m^* \xi_0}, \tag{3.2}$$

we get [29] the dimensionless BdG-equations

$$\begin{aligned} \left(\frac{-1}{2k_F\xi_0}\nabla^2 - \mathcal{E}_F \right) u_k(\mathbf{x}) + \Delta(\mathbf{x}) v_k(\mathbf{x}) &= \mathcal{E}_k u_k(\mathbf{x}), \\ -\left(\frac{-1}{2k_F\xi_0}\nabla^2 - \mathcal{E}_F \right) v_k(\mathbf{x}) + \Delta^*(\mathbf{x}) u_k(\mathbf{x}) &= \mathcal{E}_k v_k(\mathbf{x}) \end{aligned} \tag{3.3}$$

where the index k denotes all quantum numbers. With some abuse of notation, Δ is now measured in units of T_c. It is easy to show that $\mathcal{E}_F = k_F\xi_0/2$. Next,

we choose a separable form for the quasiparticle amplitudes:

$$u_k(\mathbf{x}) = u_{n\mu_u}(r)e^{i\mu_u\theta}e^{ik_z z},$$
$$v_k(\mathbf{x}) = v_{n\mu_v}(r)e^{i\mu_v\theta}e^{ik_z z} \tag{3.4}$$

where r and z are dimensionless coordinates. Since the quasiparticles are confined to the superconductor, their amplitudes must vanish at the edge of the superconductor where $r = R$: $u_{n\mu}(R) = v_{n\mu}(R) = 0$. The angular momentum quantum numbers μ_u and μ_v will depend on the properties of the superconductor, since

$$\Delta(\mathbf{x}) = \Delta(r)e^{i(\mu_u-\mu_v)\theta} \quad \text{with} \quad \Delta(r) = |\Delta(\mathbf{x})|. \tag{3.5}$$

In choosing the phase $\mu_u - \mu_v$ of the order parameter we thus determine what category of solutions to the BdG equations we look at. A real order parameter, $\mu_u - \mu_v = 0$, describes a bulk superconductor, $\mu_u - \mu_v = \pm 1$ describes a vortex containing one quantum of flux, and so on.

Expanding ∇^2 in cylindrical coordinates, the exponentials cancel and we are left with the following equations for r:

$$\left[\frac{-1}{2k_F\xi_0}\left(\frac{\partial^2}{\partial^2 r} + \frac{1}{r}\frac{\partial}{\partial r} - \frac{\mu_u^2}{r^2} - k_z^2\right) - \mathcal{E}_F\right] u_{n\mu_u} + \Delta v_{n\mu_v} = \mathcal{E}_n u_{n\mu_u},$$
$$-\left[\frac{-1}{2k_F\xi_0}\left(\frac{\partial^2}{\partial^2 r} + \frac{1}{r}\frac{\partial}{\partial r} - \frac{\mu_v^2}{r^2} - k_z^2\right) - \mathcal{E}_F\right] v_{n\mu_v} + \Delta u_{n\mu_u} = \mathcal{E}_n v_{n\mu_v}. \tag{3.6}$$

These equations can be rewritten as a matrix equation with the eigenvalue $\mathcal{E}_n$ and the eigenvector being the spinor $\psi = (u_{n\mu_u}, v_{n\mu_v})$. Following Gygi and Schlüter [8], we assume that the Fermi surface is cylindrical along the k_z-axis, in which case the quasiparticle motion will be in the plane and the k_z^2-term can be dropped. This is applicable to, for example, the cuprate superconductors [30].

To solve equation (3.6), we make a series expansion of the quasiparticle amplitudes $u_{n\mu_u}$ and $v_{n\mu_v}$:

$$u_{n\mu_u}(r) = \sum_j c_{nj}\varphi_{j\mu_u}(r),$$
$$v_{n\mu_v}(r) = \sum_j d_{nj}\varphi_{j\mu_v}(r). \tag{3.7}$$

where j runs from 0 to some $N \gg 1$. Since the problem has cylindrical symmetry, the natural choice of basis functions is the Bessel functions of the first kind, normalized in a disc of radius R:

$$\varphi_{j\mu}(r) = \varphi_{j\mu}\left(\frac{\alpha_{j\mu}}{R}r\right) = \frac{\sqrt{2}}{RJ_{\mu+1}(\alpha_{j\mu})}J_\mu\left(\frac{\alpha_{j\mu}}{R}r\right) \tag{3.8}$$

where $\alpha_{j\mu}$ is the j:th zero of J_μ. Numerical values for these can be found in Abramowitz and Stegun [31].

We note that the basis functions fulfill the boundary condition $u_{n\mu}(R) = v_{n\mu}(R) = 0$ by construction. They also form a complete orthonormal set on $[0, R]$. That

is, [28]

$$\langle \varphi_{j\mu} \ , \ \varphi_{j'\mu} \rangle = \int_0^R \mathrm{d}r \ r\varphi_{j\mu}(r)\varphi_{j'\mu}(r) = \delta_{jj'}. \tag{3.9}$$

We can easily calculate the derivatives of the basis functions:

$$\begin{aligned}
\frac{\partial \varphi_{j\mu}}{\partial r} &= \frac{\alpha_{j\mu}}{2R}\left(\varphi_{j\mu-1}\left(\frac{\alpha_{j\mu}}{R}r\right) - \varphi_{j\mu+1}\left(\frac{\alpha_{j\mu}}{R}r\right)\right), \\
\frac{\partial^2 \varphi_{j\mu}}{\partial^2 r} &= \left(\frac{\alpha_{j\mu}}{2R}\right)^2\left(\varphi_{j\mu-2}\left(\frac{\alpha_{j\mu}}{R}r\right) - 2\varphi_{j\mu}\left(\frac{\alpha_{j\mu}}{R}r\right) + \varphi_{j\mu+2}\left(\frac{\alpha_{j\mu}}{R}r\right)\right).
\end{aligned} \tag{3.10}$$

Here, we include the full argument of the Bessel function in the definition (3.8) to emphasize that we will – where derivatives have been taken – encounter basis functions on the form $\varphi_{j\nu}(\alpha_{j\mu}r/R)$ where the order μ of the zero in the argument differs from the order ν of the function.

The recurrence relations for successive Bessel functions [31] allow us to rewrite

$$\varphi_{j\nu-1}\left(\frac{\alpha_{j\mu}}{R}r\right) + \varphi_{j\nu+1}\left(\frac{\alpha_{j\mu}}{R}r\right) = \frac{R}{\alpha_{j\mu}}\frac{2\nu}{r}\varphi_{j\nu}\left(\frac{\alpha_{j\mu}}{R}r\right). \tag{3.11}$$

With our collection of mathematical tools complete, we start with the first equation of (3.6). We substitute the series expansion (3.7) and take the inner product (as defined in equation (3.9)) with $\varphi_{j'\mu_u}(r)$.

We evaluate the integrals one by one. Performing the derivatives in the first one and rearranging terms, we have

$$\begin{aligned}
&\sum_j c_{nj}\int_0^R \mathrm{d}r \ r\varphi_{j'\mu_u}\left[\frac{-1}{2k_F\xi_0}\left(\frac{\partial^2}{\partial^2 r} + \frac{1}{r}\frac{\partial}{\partial r} - \frac{\mu_u^2}{r^2}\right) - \mathcal{E}_F\right]\varphi_{j\mu_u} = \\
&\sum_j c_{nj}\int_0^R \mathrm{d}r \ r\varphi_{j'\mu_u}\Bigg[\left(\frac{1}{2k_F\xi_0}\left(\frac{\alpha_{j\mu_u}}{R}\right)^2\frac{1}{2} - \mathcal{E}_F\right)\varphi_{j\mu_u} - \frac{1}{2k_F\xi_0}\left(\frac{\alpha_{j\mu_u}}{R}\right)^2 \times \\
&\qquad \frac{1}{4}\left(\varphi_{j\mu_u-2} + \varphi_{j\mu_u+2} - \frac{R}{\alpha_{j\mu_u}}\frac{2}{r}(\varphi_{j\mu_u-1} - \varphi_{j\mu_u+1}) - \left(\frac{2R}{\alpha_{j\mu_u}}\right)^2\frac{\mu_u^2}{r^2}\varphi_{j\mu_u}\right)\Bigg]
\end{aligned} \tag{3.12}$$

The first bracketed term is a constant and can be taken outside the integral. In the second bracket, we remember that all the $\varphi_{j\nu}$ have the same argument $\alpha_{j\mu_u}r/R$, regardless of their value of ν. We use equation (3.11) to rewrite

$$\left(\frac{2R}{\alpha_{j\mu_u}}\right)^2\frac{\mu_u^2}{r^2}\varphi_{j\mu_u} = \frac{R}{\alpha_{j\mu_u}}\frac{2\mu_u}{r}\left(\varphi_{j\mu_u-1} + \varphi_{j\mu_u+1}\right). \tag{3.13}$$

Collecting terms and again making use of (3.11), the second bracket of equation (3.12) becomes

$$\varphi_{j\mu_u-2} + \varphi_{j\mu_u+2} - \frac{R}{\alpha_{j\mu_u}}\frac{2}{r}\Big((\mu_u-1)\varphi_{j\mu_u-1} + (\mu_u+1)\varphi_{j\mu_u+1}\Big) = -2\varphi_{j\mu_u} \tag{3.14}$$

and the whole expression is

$$\begin{aligned}\sum_j c_{nj}\left(\frac{1}{2k_F\xi_0}\left(\frac{\alpha_{j\mu_u}}{R}\right)^2-\mathcal{E}_F\right)\int_0^R \mathrm{d}r\ r\varphi_{j'\mu_u}\varphi_{j\mu_u}\\ =\sum_j c_{nj}\left(\frac{1}{2k_F\xi_0}\left(\frac{\alpha_{j\mu_u}}{R}\right)^2-\mathcal{E}_F\right)\delta_{jj'}\\ =c_{nj'}\left(\frac{1}{2k_F\xi_0}\left(\frac{\alpha_{j'\mu_u}}{R}\right)^2-\mathcal{E}_F\right).\end{aligned} \tag{3.15}$$

The second integral is

$$\sum_j d_{nj}\int_0^R \mathrm{d}r\ r\varphi_{j'\mu_u}\Delta(r)\varphi_{j\mu_v} \tag{3.16}$$

which cannot be solved without knowing something about $\Delta(r)$, and the right-hand side is

$$\sum_j c_{nj}\int_0^R \mathrm{d}r\ r\varphi_{j'\mu_u}\mathcal{E}_{n\mu}\varphi_{j\mu_v}=c_{nj'}\mathcal{E}_n. \tag{3.17}$$

In the same way, only taking the inner product with $\varphi_{j'\mu_v}(r)$ this time, the second equation of (3.6) becomes

$$-d_{nj'}\left(\frac{1}{2k_F\xi_0}\left(\frac{\alpha_{j'\mu_v}}{R}\right)^2-\mathcal{E}_F\right)+\sum_j c_{nj}\int_0^R \mathrm{d}r\ r\varphi_{j'\mu_v}\Delta^*(r)\varphi_{j\mu_u}=d_{nj'}\mathcal{E}_n. \tag{3.18}$$

Since we get similar equations for each value of j', we may gather the coefficients in a vector $\Psi_n=(c_{n,1},\ldots,c_{n,N},d_{n,1},\ldots,d_{n,N})$ (that is, $j=1,2,\ldots,N$) and rewrite equations (3.6) as an eigenvalue problem:

$$\begin{pmatrix} T^u & D\\ D^T & -T^v\end{pmatrix}\Psi_n=\mathcal{E}_n\Psi_n. \tag{3.19}$$

$T^{u,v}$ is diagonal with elements

$$T^{u,v}_{jj}=\frac{1}{2k_F\xi_0}\left(\frac{\alpha_{j\mu_{u,v}}}{R}\right)^2-\mathcal{E}_F, \tag{3.20}$$

which we realize are the normal state-energies $\xi_{j\mu}$, now in units of T_c. D has elements

$$\begin{aligned}D_{j'j}&=\int_0^R \mathrm{d}r\ r\varphi_{j'\mu_u}(r)\Delta(r)\varphi_{j\mu_v},\\ D^T_{j'j}&=\int_0^R \mathrm{d}r\ r\varphi_{j'\mu_v}(r)\Delta(r)\varphi_{j\mu_u}.\end{aligned} \tag{3.21}$$

The eigenvalue equation (3.19) is central to the numerical solution. The process is described in algorithm 2 in section 3.2.2

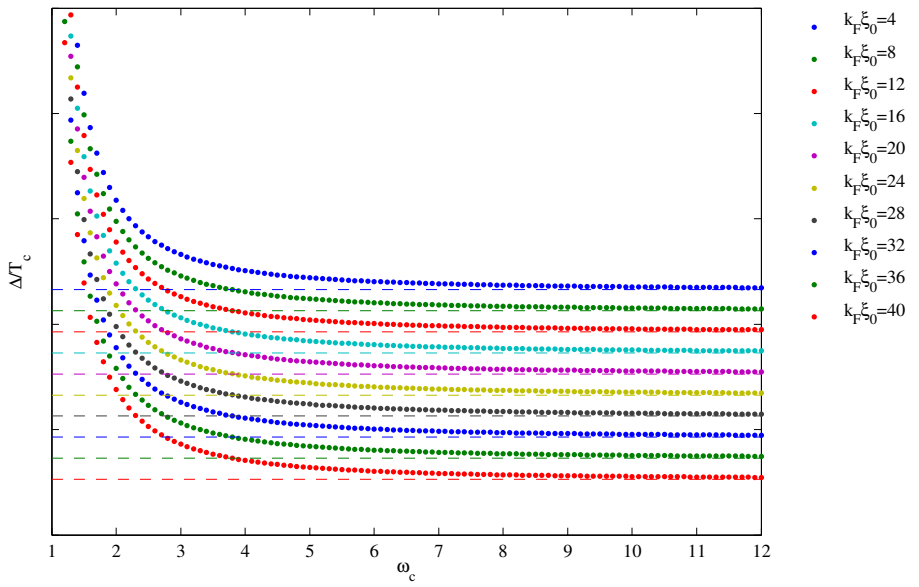

Figure 3.1: Illustration of the divergence of Δ_∞ with decreased ω_c. The plots have been shifted vertically for clarity: the dashed lines are the correspondingly shifted BCS predictions.

3.1.1 Eliminating cut-off dependence

We note that the gap equation (2.35) diverges logarithmically with ω_c. This is undesirable, and we may avoid this difficulty by switching to an effective coupling constant g_{eff}. We rewrite (2.36) as

$$\frac{1}{g} - \sum_k \frac{1}{2\xi_k} \tanh\left(\frac{\xi_k}{2T}\right) = \sum_k \frac{1}{2\mathcal{E}_k} \tanh\left(\frac{\mathcal{E}_k}{2T}\right) - \sum_k \frac{1}{2\xi_k} \tanh\left(\frac{\xi_k}{2T}\right). \quad (3.22)$$

Since $\mathcal{E}_k \to \xi_k$ as k goes to infinity, the right-hand side of this expression converges to zero. We transform the sums over ξ_k to integrals, and evaluate the one on the left similarily to that in equation (2.37). Using the result (2.38), we can then define

$$\frac{1}{g_{eff}} = \ln\frac{T}{T_c} + \int_0^{\omega_c} \mathrm{d}\xi \; \frac{1}{\xi} \tanh\left(\frac{\xi}{2T}\right) \quad (3.23)$$

Here, we have absorbed the factor $N(0)$ in g_{eff} so that the coupling constant is dimensionless. The self-consistency equation becomes

$$\Delta = g_{eff} \sum_n \frac{\Delta}{2\mathcal{E}_k} \tanh\left(\frac{\mathcal{E}_k}{2T}\right), \quad (3.24)$$

or, from equation (2.33),

$$\Delta = g_{eff} \sum_k u_k v_k^* \tanh\left(\frac{\mathcal{E}_k}{2T}\right). \quad (3.25)$$

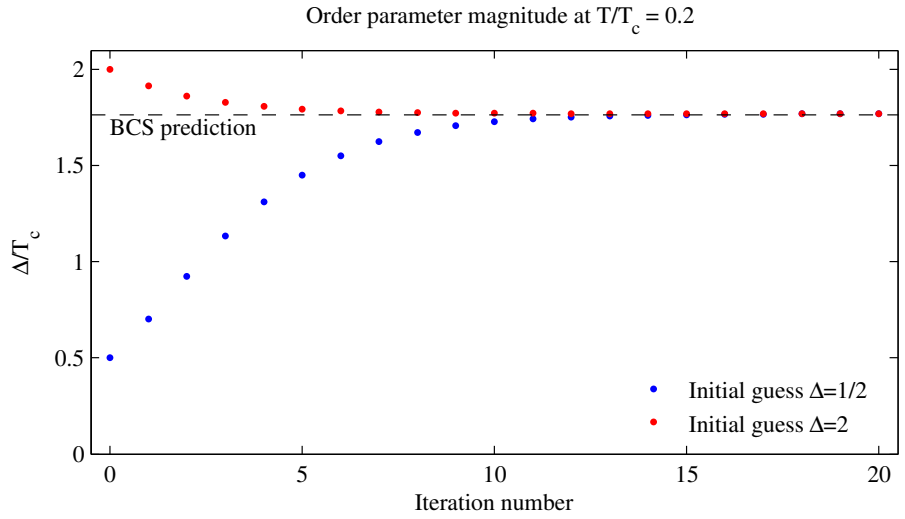

Figure 3.2: Convergence of Δ_∞ calculated according to algorithm 1 as a function of the number of iterations, for initial values $\Delta_{in} = 1/2$ and 2.

We still need to choose a cut-off energy ω_c, but the sum over $|\mathcal{E}_k| \leq \omega_c$ will not depend on the exact value. We pay for this by limiting our model to temperatures $0 < T/T_c < 1$.

This procedure fails for very small values of ω_c, since $\ln(T/T_c) < 0$. The sum in equation (3.23) only runs over $|\xi_k| < \omega_c$, so a small enough ω_c might give a negative effective coupling constant. In figure 3.1, the order parameter magnitude as calculated in section 3.2.1 is shown as a function of cut-off frequency. We see that we do indeed get a divergence where Δ_∞ is overestimated if ω_c is chosen too small. For large $k_F\xi_0$, reasonable agreement with theory is easy to obtain by choosing an appropriate ω_c. However, since we cannot choose the cut-off energy to be larger than $\mathcal{E}_F = k_F\xi_0/2$ it is not possible to choose an ω_c which is "large enough" for small $k_F\xi_0$. We thus expect the order parameter to be overestimated in this limit.

3.2 Order parameter in a bulk superconductor

In order to make sure our method does what it is supposed to do, we will start with a bulk superconductor - a spatially homogenous material where no vortices are present. In this case, $\Delta(\mathbf{x})$ is real. Then, by equation (3.5), $\mu_u = \mu_v = \mu \in \mathbb{Z}$ and the matrix D reduces to an identity matrix.

We split this problem into two parts. First, we find the magnitude of the gap in a single point to make sure the numerical solution converges appropriately. Second, we include the r-dependence and solve the eigenvalue problem described above, making sure that it returns a constant $\Delta(r)$. Henceforth we use $R = 100$.

3.2.1 Convergence of magnitude

To begin with, the ξ_k were chosen to be uniformly distributed between 0 and ω_c; since the integral in equation (3.23) is even in ξ_n the negative energies contribute a factor 2. To remove the divergence at $\xi_k = 0$ we shift the energies into the complex plane: $\xi_k \to \xi_k + i0$ where $i0$ denotes an infinitesimally small imaginary part. The sums were transformed into integrals, and the gap was calculated with algorithm 1. Initial guesses of $\Delta_{in} = 0.5$ and 2.0 were tried, and convergence was found within twenty iterations; see figure 3.2.

The next step is to replace the linear energy spectra with that given by equation (3.20). There are now two indicies labeling the energies, and implementation of algorithm 1 is not entirely straightforward. We deal with this by stepping through all the values of μ and collecting those $\xi_{j\mu}$ that are in the interval $\mathcal{E}_F \pm \omega_D$ in a single vector; this replaces line 1 in algorithm 1. The rest of the calculation is unchanged from before. As expected, the results are similar to those using the linear spectra.

Algorithm 1: Self-consistent calculation of the magnitude of the order parameter

Input: initial guess Δ_{in}, cut-off ω_c, temperature T
Output: self-consistently calculated Δ_{out}

```
Define the spectrum ξ + i0                                   1
Calculate g_eff with equation (3.23)                         2
while convergence not found do                               3
    Calculate E = sqrt(ξ^2 + Δ_in^2)                         4
    Calculate Δ_out with equation (3.24)                     5
    if |Δ_in − ℜ(Δ_out)| < tolerance then                    6
        convergence found                                    7
    else                                                     8
        Δ_in ← ℜ(Δ_out)                                      9
    end if                                                   10
end while                                                    11
```

3.2.2 Radial dependence

Having fixed the magnitude of the order parameter, we wish to solve for the r-dependence in a bulk superconductor before including the vortex by switching to a complex Δ. This means employing the full machinery developed in section 3.1. The process is described in algorithm 2 on page 24, but we replace lines 10–13 with the assignment $D = \mathbb{1}$.

Since both matrices T and D are diagonal, there are only two non-zero components in each eigenvector Ψ_n: one coefficient c_{nm} and one d_{nm} for some m. Thus, each $u_{n\mu}, v_{n\mu}$ only contains a single basis function $\varphi_{\mu m}$ and $u_{n\mu}v^*_{n\mu} \propto J^2_\mu$. If we replace $\mu \to -\mu$, we have $u_{n\mu}v^*_{n\mu} \propto J^2_{-\mu} = ((-1)^\mu J_\mu)^2 = J^2_\mu$ since we have chosen μ to be integer. That is, the sum over $\mu < 0$ introduces a degeneracy

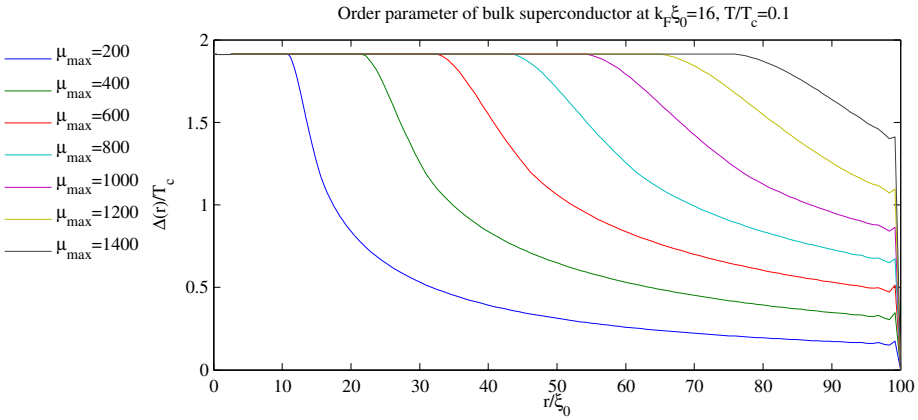

Figure 3.3: Order parameter calculated for different values of μ_{max}. The cut-off was chosen as $\omega_c = \mathcal{E}_F/3 = 8/3$, and the overestimation of Δ_∞ is exactly as big as we expect – recall fig. 3.1 and discussion thereof.

factor 2. As we perform the sum in equation (3.24), we thus realize that

$$\Delta \propto J_0^2 + 2\sum_{\mu=1}^{\infty} J_\mu^2 = 1, \tag{3.26}$$

where the equality is a known Bessel function identity [31]. Of course, we do not in practice sum over an infinite number of μ, but equation (3.26) gives us an indication that it is indeed possible to calculate a constant order parameter in our framework.

As we can see in figure. 3.3, we do indeed succeed in reproducing the constant order parameter of a bulk superconductor, as well as the expected gapped energy spectra. For the r-dependence of the order parameter, the number of μ in the sum is crucial. We understand this by looking at some sample quasiparticle amplitudes $u_{n\mu}$ and $v_{n\mu}$, as shown in figure 3.4. We see that higher μ increase the inner radius for which the wave function is zero. That is, only a comparably small number of wave functions contribute to the behaviour of the order parameter near the origin, and the rest only serve to "fill out" the rest of the domain. We will make use of this fact when calculating the vortex state in section 3.3.

Two optimization points in algorithm 2 remain to be discussed. First, we explain why on line 7 we compare the normal state energies rather than the calculated eigenvalues with ω_c and second, we comment on the input variables.

As we have seen in equation (3.21), in general the elements of D require numerical integration – a slow process. It turns out that the total time it takes to calculate D and solve the $2N \times 2N$ eigenvalue problem (3.19) scales as N^2. Thus, by limiting N as much as possible we can cut down significantly on computation time. This can be done by noting that the condition $|\xi_n| < \omega_c$ is equivalent to $|\mathcal{E}_n| < \sqrt{\omega_c^2 + |\Delta|^2}$; a simple shift in cut-off frequency for the quasiparticle energies. Since the gap equation is now independent of ω_c, this is permissible.

Using $|\xi_n| < \omega_c$ instead of $|\mathcal{E}_n| < \omega_c$ means that we sort out which energies to

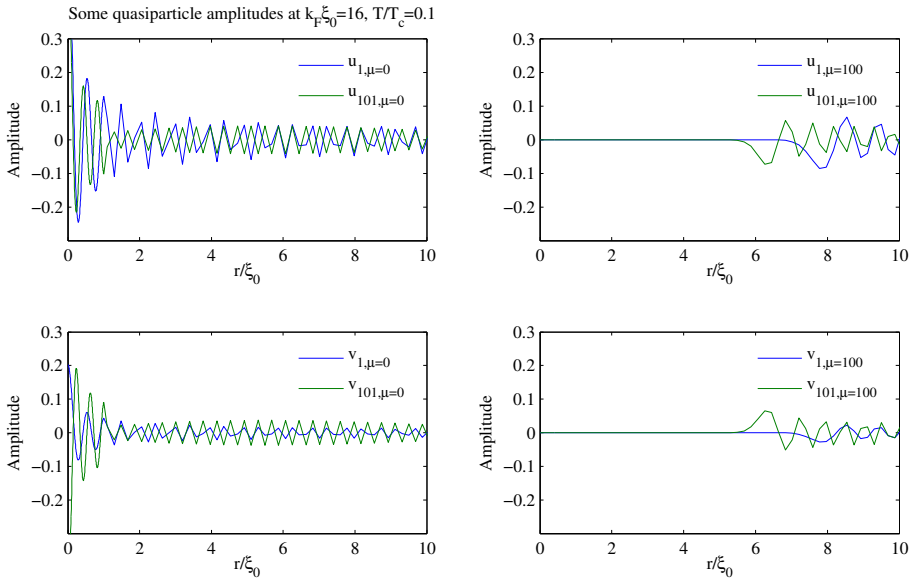

Figure 3.4: Quasiparticle amplitudes for various parameter values. Note how those corresponding to higher values of μ are zero in a region near the origin.

keep in the sum in equation (2.33) before we solve the eigenvalue problem. In practice, we calculate the normal state energies

$$\xi_{j\mu} = \frac{1}{2k_F\xi_0}\left(\frac{\alpha_{j\mu}}{R}\right)^2 - \mathcal{E}_F, \tag{3.27}$$

and determine how many of these lie within the cut-off frequency. This gives us the size of the T- and D-matrices. Implementing the cut-off in this way means that we sum over all the resulting eigenvalues $\mathcal{E}_{j\mu}$. The validity of the shift in cut-off frequency is supported by figure 3.5. Here, the positive branch of the eigenvalues calculated in this way are plotted together with the energies $\mathcal{E}_{j\mu} = \sqrt{\xi_{j\mu}^2 + |\Delta|^2}$; the correspondence is indeed very good.

Finally, we note that we rely on calculating and tabulating the basis functions $\varphi_{j\mu}$ in advance. This is common sense: typical values are $j, \mu_{max} \sim 10^2$ and the interval $[0, R]$ divided into 500 grid points – we then need to evaluate 10^4 Bessel functions in 500 points each. By pre-tabulating these values we can do away with this step in advance instead of repeating it each time we iterate over line 2, algorithm 2; a speed-up of a factor 10^2. The matrix D^{const} will be discussed in section 3.3.

3.3 The vortex phase

We now move on to the main subject of this thesis: the vortex phase of an s-wave superconductor. A very crude approximation of a vortex is a deep potential well. From basic quantum mechanics [18] we expect particles to be trapped in

Algorithm 2: Self-consistent calculation of the r-dependent order parameter near a vortex line. Once $\Delta(r)$ has been determined, single evaluations of lines 6–16 for a given μ allow us to extract the energy spectrum and the wave functions $u_{n\mu}, v_{n\mu}$ of a particular state.

Input: initial guess Δ_{in}, cut-off ω_c and μ_{max}, temperature T, tabulated values for the matrix D^{const} and the basis functions $\varphi_{j\mu}$
Output: self-consistently calculated Δ_{out}, optional: supercurrent j_θ

```
Calculate g_eff with equation (3.23)                                          1
while convergence not found do                                                2
    Initialize Δ_out ← 0                                                      3
    Optional: initialize j_θ ← 0                                              4
    for μ_{u,v} = −μ_max to μ_max do                                          5
        Calculate the spectrum ξ_{jμ_{u,v}} + i0 with equation (3.27)         6
        Discard all ξ_{jμ_{u,v}} such that |ξ_{jμ_{u,v}}| < ω_c               7
        Note the values of j for the remaining ξ_{jμ_{u,v}}                   8
        Create the matrix T^{u,v}: T^{u,v}_{jj} = ξ_{jμ_{u,v}}                9
        Pick out the corresponding (same values of μ and j, j′) matrix        10
          D^const from the tabulated values                                   11
        Calculate D^corr with equation (3.28)                                 12
        Form D = D^const + D^corr                                             13
        Solve equation (3.19) for the eigenvectors Ψ and the eigenvalues E    14
        for each eigenvalue E_n do                                            15
            Calculate u_n and v_n with equation (3.7)                         16
            Update Δ_out ← Δ_out + g_eff u_{nμ} v*_{nμ} tanh(E_n/2T)          17
            Optional: update j_θ ←                                            18
              j_θ + f(E_n)|u_{nμ}|²(μ − 1/2) − (1 − f(E_n))|v_{nμ}|²(μ + 1/2)  19
        end for                                                               20
    end for                                                                   21
    if |Δ_in − ℜ(Δ_out)| < tolerance then                                     22
        convergence found                                                     23
    else                                                                      24
        Δ_in ← ℜ(Δ_out)                                                       25
    end if                                                                    26
end while                                                                     27
```

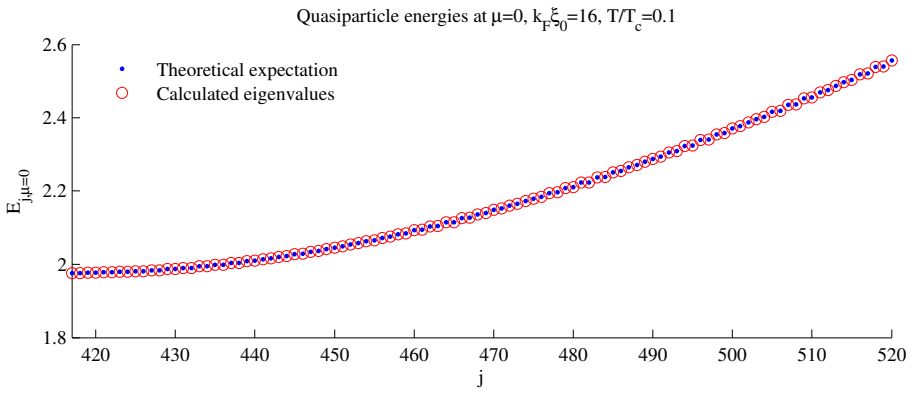

Figure 3.5: Comparison of quasiparticle energies of a bulk superconductor calculated from the eigenvalue problem (3.19) and the $\mathcal{E}_{j\mu} = \sqrt{\xi_{j\mu}^2 + |\Delta|^2}$ *expected from theory.*

such a well, and that they occupy a set of discrete energy levels. This does in fact happen in a vortex core, as verified by scanning tunneling microscopy-experiments [32, 33]. The localized states have been predicted [5] to have a level spacing of $\mu\Delta_\infty/\mathcal{E}_F$. For a spin singlet superconductor like the s-wave we are working with, $|\mu| = 1/2, 3/2, 5/2\ldots$, so there is no state at the Fermi energy with $\mathcal{E} = 0$. The energy of the lowest state is called the minigap.

We will look at four quantities: the order parameter to compare with existing results, the supercurrent around the vortex as an example of a physical observable predicted by the model, the spectrum of quasiparticle energies and the spatial location of the vortex core states. The method is described in algorithm 2. We are in particular interested in the low temperature-limit where $T/T_c \ll 1$, and thus postpone discussion of the results to section 3.4. For the remainder of this section, we discuss some matters of implementation.

As we saw in section 3.1, we introduce a vortex in our calculation by choosing a phase for the order parameter. Here, we set $\Delta(\mathbf{x}) = \Delta(r)e^{-i\theta}$ where the magnitude $\Delta(r)$ is real. It follows that $\mu_u - \mu_v = -1$; for simplicity we set $\mu_u = \mu - 1/2$ and $\mu_v = \mu + 1/2$, where $|\mu| = 1/2, 3/2, 5/2\ldots$

As we have seen in section 3.2.2, a large number of angular momentum quantum numbers μ are required to achieve a constant order parameter in the entire domain. In principle, $\mu \to \infty$. We must choose a maximum value for μ in a clever way. With a little thought, we realize that we can use our knowledge of the order parameter to set μ_{max} and in the process decrease the number of computations required. Namely, we know that the order parameter magnitude $\Delta(r) = \Delta_\infty$ far from the vortex, so it suffices to calculate the deviation from the constant Δ_∞ for small r. This allows us to greatly reduce the number of μ:s involved.

Recalling figure 3.4, we see that for large μ all $u_{n\mu}(r)$ and $v_{n\mu}(r)$ are zero near the origin and can be safely excluded without any loss of information regarding the relevant region. Thus, treating the problem as a matter of corrections at

small r rather than a matter of summing to a constant at large r means that we only include those μ that do give eigenfunctions which are non-zero close to $r = 0$. This means a decrease of about a factor 10 in the number of μ:s – and hence the computation time – required.

In practice, we split the matrix D into two parts: $D = D^{const} + D^{corr}$. The constant part D^{const} is calculated with equation (3.21) using $\Delta(r) = \Delta_\infty$: this calculation can be done once and for all instead of re-calculating D every time we update $\Delta(r)$. The correction

$$D^{corr}_{j'j} = \int_0^a \mathrm{d}r\; r\varphi_{j'\mu_u}(r)\big(\Delta(r) - \Delta_\infty\big)\varphi_{j\mu_v}(r) \tag{3.28}$$

has to be calculated each iteration. However, the integrand $\Delta(r) - \Delta_\infty$ goes to zero within a few ξ_0, so we may take the upper integration limit $a \ll R$. It follows that μ_{max} is chosen such that $u_{n\mu_{max}}(r) = v_{n\mu_{max}}(r) = 0$ for $0 < r < a$. In the calculations, we set $\Delta(r) = \Delta(a)$ for $a < r < R$.

As mentioned in section 2.2.2, the BdG equations are unchanged when transforming $(u_k, v_k) \to (-v_k^*, u_k^*)$ and $\mathcal{E}_k \to -\mathcal{E}_k$ simultaneously. From equation (3.4);

$$\begin{aligned} u_k^* &= u_{n\mu} e^{-i(\mu-1/2)\theta} \overset{\mu\to-\mu}{\longrightarrow} u_{n\mu} e^{i(\mu+1/2)\theta} \\ v_k^* &= v_{n\mu} e^{-i(\mu+1/2)\theta} \overset{\mu\to-\mu}{\longrightarrow} v_{n\mu} e^{i(\mu-1/2)\theta}. \end{aligned} \tag{3.29}$$

That is, the corresponding transformation of the r-dependent equations (3.6) is to change the sign of $\mathcal{E}_k$ and switch the roles of $\mu_u = \mu - 1/2$ and $\mu_v = \mu + 1/2$. However, this assumes that the states are symmetrically distributed around the Fermi level and thus enforces a particle-hole symmetry. As we can see in figure 3.6, this is not always the case. For low $k_F\xi_0$, the relevant selection of energies is no longer uniformly distributed and there will be more states included below $\mathcal{E}_F$ than above.

The particle-hole asymmetry can be seen in density of states-calculations and -experiments [29, 34], but only affects the order parameter marginally. This is because the u_k and v_k are paired together when calculating Δ, so the same oscillatory components are included for μ as for $-\mu$. We make a qualitative argument by looking at $\mu = \pm 1/2$.

Using the series expansion (3.7) we find the n:th corresponding quasiparticle amplitudes

$$\begin{aligned} u_{n,0} &= \sum_j c_{nj}\varphi_{j,0}, & u_{n,-1} &= \sum_j c_{nj}\varphi_{j,-1}, \\ v_{n,1} &= \sum_j d_{nj}\varphi_{j,1}, & v_{n,0} &= \sum_j d_{nj}\varphi_{j,0} \end{aligned} \tag{3.30}$$

where the left column correspond to $\mu = 1/2$ and the right to $\mu = -1/2$. All basis functions with the same second index will be oscillating within an exponentially decreasing envelope function, call it V_0. Since $u_{n,0}$ and $v_{n,0}$ are proportional to the same basis functions they thus look qualitatively the same, possibly

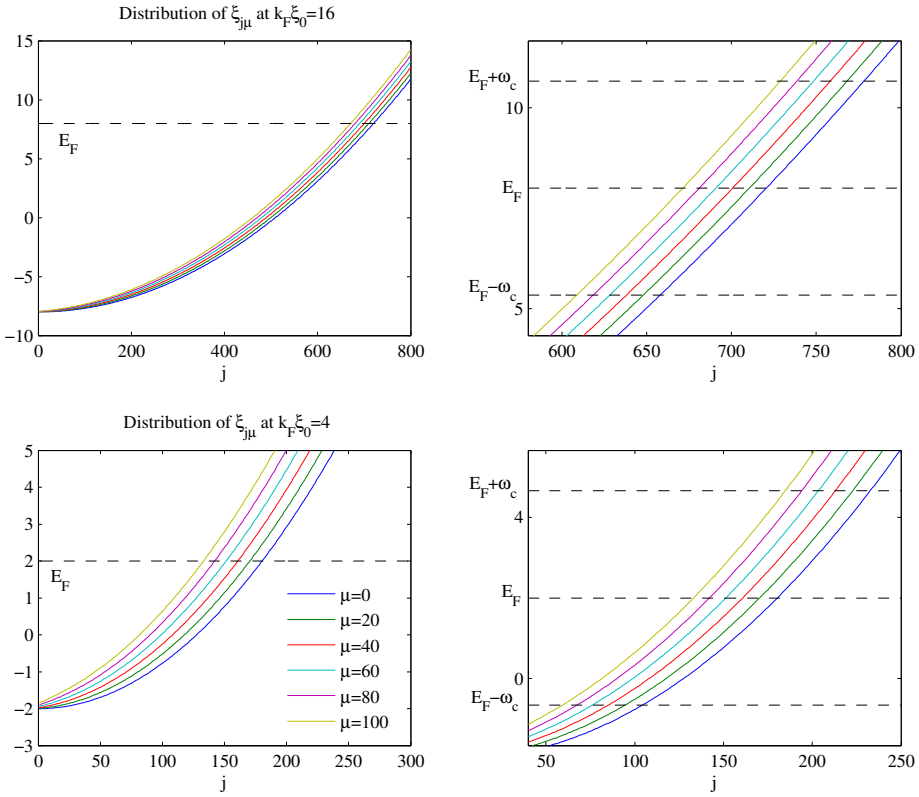

Figure 3.6: Illustration of the normal-state energies $\xi_{j\mu}$ for two values of $k_F\xi_0$. The right panels are magnifications of the area where the Fermi energy $\mathcal{E}_F$ intersects the parabolas, with the cut-off frequency ω_c included.

up to a constant k_0. The same is true for $u_{n,-1}$ and $v_{n,1}$ since $J_{-1} = -J_1$ (so $k_1 < 0$). The contribution to Δ from $\mu = 1/2$ is then

$$g_{\mathit{eff}} u_{n,0} v_{n,1} \tanh(\mathcal{E}_{n,1/2}/2T) \propto k_0 V_0 V_1, \tag{3.31}$$

and from $\mu = -1/2$

$$g_{\mathit{eff}} u_{n,-1} v_{n,0} \tanh(-\mathcal{E}_{n,1/2}/2T) \propto -k_1 V_1 V_0 \tag{3.32}$$

where the minus sign comes from $\tanh(-\mathcal{E}) = -\tanh(\mathcal{E})$. With the normalization condition $|u_k|^2 + |v_k|^2 = 1$ we find that

$$k_0^2 = \frac{1 - |u_{n,0}|^2}{|u_{n,0}|^2} = \frac{|v_{n,0}|^2}{1 - |v_{n,0}|^2} \tag{3.33}$$

and similarly for k_1. For low energies, $|u_{n,0}|^2 \approx |v_{n,0}|^2 \approx 1/2$ (see figure 2.1), in which case $k_0 \approx -k_1 \approx 1$.

We can then neglect particle-hole asymmetry when calculating the order parameter. A given positive μ then contributes a term

$$g_{\mathit{eff}} u_{n\mu} v_{n\mu}^* \tanh(\mathcal{E}_{n\mu}/2T) \tag{3.34}$$

to the sum in equation (3.25), and the corresponding negative $-\mu$ contributes an identical term:

$$g_{\mathit{eff}} (-v_{n\mu}^*)(u_{n\mu}^*)^* \tanh(-\mathcal{E}_{n\mu}/2T) = g_{\mathit{eff}} u_{n\mu} v_{n\mu}^* \tanh(\mathcal{E}_{n\mu}/2T). \tag{3.35}$$

It is clear that we can limit the sum on line 5 of algorithm 2 to non-negative μ and compensate with a degeneracy factor 2.

3.3.1 Supercurrent density

A theory is no better than its capability to predict experimental results. One physical observable that we can measure is the current. As mentioned in chapter 2, the density of superconducting electrons is related to the GL wave function as $n_s = |\psi|^2$. It is then natural to identify the supercurrent with the probability current [18]:

$$\mathbf{j}(\mathbf{r}) \propto -i \left(\psi^\dagger \nabla \psi - (\nabla \psi^\dagger) \psi \right). \tag{3.36}$$

This result is easily derived by minimizing the Ginzburg-Landau free energy with respect to the order parameter [23]. We extend equation (3.36) to our spinor $\psi = (u_k(\mathbf{r}), v_k(\mathbf{r}))$ as [8]

$$\begin{aligned} \mathbf{j}(\mathbf{r}) \propto -i \sum_k \Big[& f(E_k) \Big(u_k^*(\mathbf{r}) \nabla u_k(\mathbf{r}) - u_k(\mathbf{r}) \nabla u_k^*(\mathbf{r}) \Big) \\ & + \Big(1 - f(E_k) \Big) \Big(v_k(\mathbf{r}) \nabla v_k^*(\mathbf{r}) - v_k^*(\mathbf{r}) \nabla v_k(\mathbf{r}) \Big) \Big]. \end{aligned} \tag{3.37}$$

This makes intuitive sense; we have the sum of the probability current for u_k and v_k, weighted by the Fermi distribution $f(E_k)$ which determines how likely

it is that a created excitation is electron-like or hole-like. Looking at the j_θ-component (the currents encircling the vortex) and using the separable form (3.4), we find

$$j_\theta(r) \propto \frac{1}{r}\sum_k \Big[f(E_k)|u_k|^2(\mu - 1/2) - \big(1 - f(E_k)\big)|v_k|^2(\mu + 1/2)\Big]. \qquad (3.38)$$

Again, k represents all quantum numbers. This is straightforward to implement, and as we shall see the calculated current shows the expected $1/r$-dependence.

3.3.2 Low temperature-limit

We wish to study the level separation of the quasiparticle states in the vortex core. In order to experimentally observe discrete energy levels, the temperature must be so low that thermal smearing of energy levels is smaller than the level spacing. As we have already mentioned, the level spacing of vortex core states in a superconductor is expected to be of order $\Delta_\infty/\mathcal{E}_F$ [5] which, up to a constant of order unity, is equal to $1/k_F\xi_0$. We thus study the regime where

$$\frac{T}{T_c} \leq \frac{1}{k_F\xi_0}. \qquad (3.39)$$

This condition is fulfilled at a low enough temperature for any material, but will be much easier to achieve experimentally for materials where the parameter $k_F\xi_0$ is small: for example the high-T_c compounds. For $NbSe_2$, on which Gygi and Schlüter [8] base their choice of parameter values, the condition (3.39) is fulfilled below 50 mK. In contrast, in the cuprate YBCO the corresponding temperature is about 10 K [29].

Decreasing $k_F\xi_0$ means that we move into a regime where Δ_∞ is of the same order as the Fermi energy. This gives us another perspective on the particle-hole asymmetry discussed above: we imagine the gap as a forbidden region around the cylindrical Fermi surface in **k**-space. All states that normally would have occupied this region are "pushed out" and end up at energies right above or below the gap. If Δ_∞ is much smaller than $\mathcal{E}_F$, the surfaces $\mathcal{E}_F + \Delta_\infty$ and $\mathcal{E}_F - \Delta_\infty$ are approximately equal and the density of states above and below the gap is similar. If $\Delta_\infty \sim \mathcal{E}_F$ this is no longer true, and the states which are being pushed into the Fermi cylinder will be packed together more closely than those pushed away from it.

We recall that the quasiparticle energies can be written

$$\mathcal{E}_{j\mu} = \sqrt{\xi_{j\mu}^2 + \Delta^2}, \qquad (3.40)$$

so the level spacing of the quasiparticle states will be determined by the spacing of the normal state levels $\xi_{j\mu}$. Using the asymptotic form [28]

$$\alpha_{j\nu} \approx j\pi + \left(\nu - \frac{1}{2}\right)\frac{\pi}{2}, \qquad (3.41)$$

we can estimate the normal state level spacing:

$$\xi_{j'\mu'} - \xi_{j\mu} = \frac{\pi^2}{2k_F\xi_0 R^2}\left(\left(j' + \frac{\mu'}{2}\right)^2 - \left(j + \frac{\mu}{2}\right)^2 - \frac{1}{4}(\mu' - \mu)\right). \qquad (3.42)$$

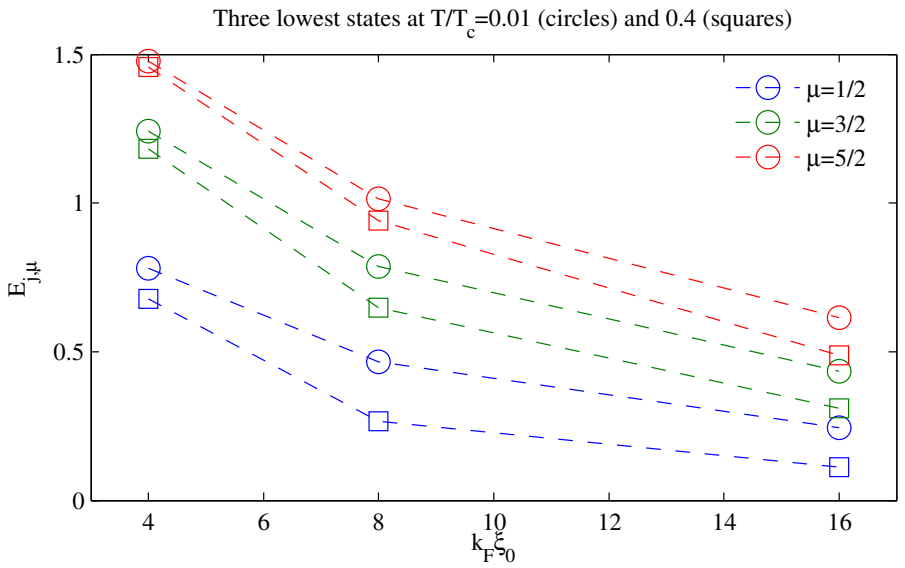

Figure 3.7: Quasiparticle energy as a function of $k_F\xi_0$ for different μ and T. We see the expected increased in level spacing with lowered temperature as well as with lowered $k_F\xi_0$.

In particular, for consecutive indicies – when $j' = j+1, \mu' = \mu$ and when $j' = j, \mu' = \mu + 1$ – the level spacing is

$$\xi_{j+1,\mu} - \xi_{j\mu} = \frac{\pi^2}{2k_F\xi_0 R^2}\,(2j + 1 + \mu) \tag{3.43}$$

respectively

$$\xi_{j,\mu+1} - \xi_{j\mu} = \frac{\pi^2}{2k_F\xi_0 R^2}\left(j + \frac{1}{2}\mu\right). \tag{3.44}$$

The bracketed term is of order 10^2, since for low-lying states $\mu \sim 10^0$ and $j \sim 10^2$ (see figure 3.6).

We note that in our formulation of the problem, we pick up an R-dependence of the level spacing; if R is decreased the level spacing will increase, and we may resolve discrete energy levels. This is the familiar mesoscopic limit present in all systems. The complication of this is that we measured R is units of ξ_0, so in decreasing $1/k_F\xi_0$ we do, in effect, shrink the domain size as well. In our results, then, the present effects are due to a combination of the low T-limit and the mesoscopic limit.

3.4 Results and discussion

We self-consistently solve the BdG-equations for material parameters $k_F\xi_0 = 4, 8,$ and 16: from section 3.2.1 we recall that we may see an overestimation of the asymptotic value Δ_∞. In each case look at temperatures $T/T_c = 0.01, 0.2, 0.4, 0.6$.

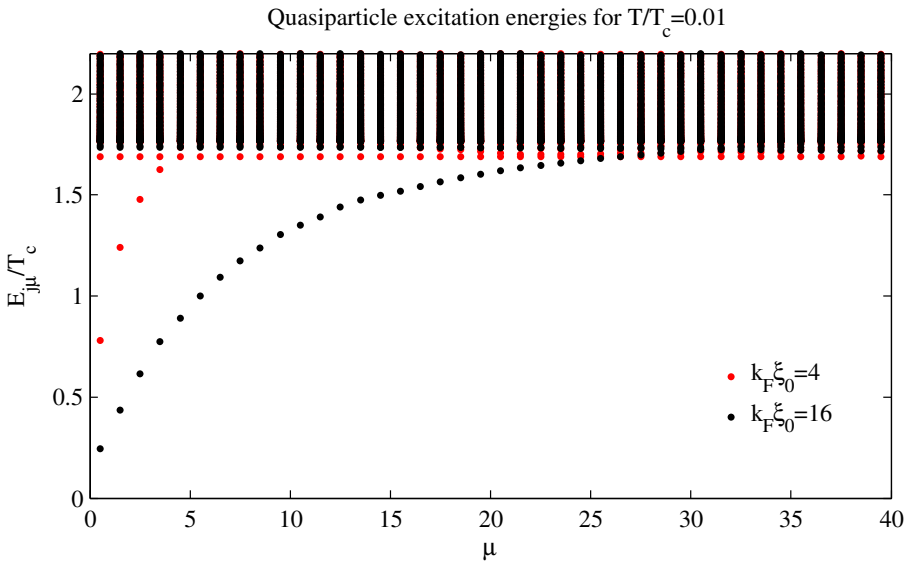

Figure 3.8: Distribution of quasiparticle energies as a function of angular momentum quantum number μ. Compare with figure 3 in the paper by Gygi and Schlüter [8]: there is good qualitative agreement, and the differences can be explained by our use of a different scale and different parameter values.

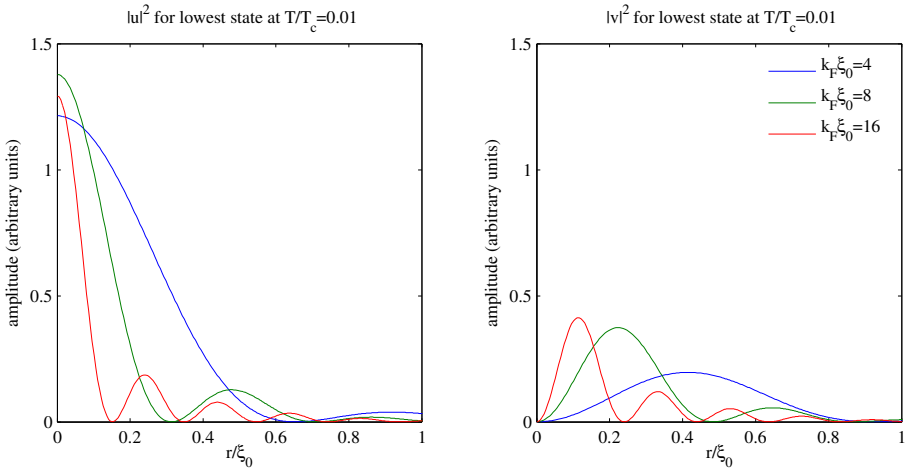

Figure 3.9: Spatial variation of the lowest core states (real part), given by $\mu = 1/2$. We see that these states are very localized.

For each set of parameter values calculations were iterated until the change in $\Delta(r)$ between iterations was smaller than 10^{-7} at every point. Here, we look at some of the results. We mention that the rate of convergence is exponential, but do not dwell on the matter.

To start with, we have plotted the energy of the three lowest states in figure 3.7, for $T/T_c = 0.01$ and 0.4. We see that lowering $k_F\xi_0$ increases the level spacing and the energy eigenvalue, whereas lowering T only increases the energy eigenvalue with roughly the same spacing. The increased minigap – the energy of the lowest state – means that there will be fewer states located in the vortex core as we approach the low T-limit. The exact number of vortex core states present at $T = 0$ is material dependent: one state for each $|\mu| = 1/2, 3/2, 5/2 \ldots$ such that $\mu\Delta_\infty/\mathcal{E}_F$ lies within the energy gap [5]. By a "vortex core state" or simply a "core state" we mean a quasiparticle state whose energy is lower than the BCS energy gap Δ_∞.

The reduction of the number of core states is further supported by figure 3.8, where we have plotted the positive energy eigenvalues as a function of the angular momentum at $T/T_c = 0.01$. We find a branch of core states for low angular momenta, which eventually joins a band of densely packed energy levels, in good agreement with previous results [8]. The length of this branch gives us the number of vortex core states.

Having established that there will be much fewer vortex core states in the low temperature-limit, we now explore the consequences of this. We know that the order parameter (equation (3.25)) and the supercurrent (equation (3.38)) are linear combinations of products between quasiparticle amplitudes. These amplitudes in turn are linear combinations of oscillating Bessel functions. As we can see in figure 3.9, the lowest core states given by $\mu = 1/2$ oscillate with a wavelength roughly proportional to $1/k_F\xi_0$. Note also that these states are spatially very localized; they are indeed *core* states.

A similar oscillatory behaviour is seen also in the states with higher energy. However, as we expect from figure 3.4, states with a higher μ – and thus higher energy – will be zero in a region around the vortex core. It follows that the order parameter and supercurrent in and near the core primarily depends on the core states. If there are many such states, the different oscillations will interfere with each other and we expect that no single quasiparticle states are discernible. On the other hand, if there are just a few core states, the oscillatory behaviour might be noticeable in the order parameter or the supercurrent.

This is indeed what happens, as we can see in figure 3.10. Here we have plotted the order parameter and supercurrent profiles for $k_F\xi_0 = 4, 8, 16$ and temperatures $T/T_c = 0.01, 0.2, 0.4, 0.6$, in a region very close to the vortex line. For the lower values of $k_F\xi_0$ we see an overestimation of the asymptotic value Δ_∞, as expected from section 3.1.1. We set the cut-off frequency to $\omega_c = 3$; if $\mathcal{E}_F = k_F\xi_0/2 < 3$ the cut-off $\omega_c = \mathcal{E}_F$ was used.

We see several expected features in the order parameter, like the overall shape similar to $\Delta(r) = \Delta_\infty \tanh(r)$ [10] and the shrinkage of the core radius with decreasing temperature [8]. However, the shrinkage of the core size saturates at low $k_F\xi_0$ and the order parameter loses the dependence on temperature. This is in agreement with previous results [29]. However, the most striking feature

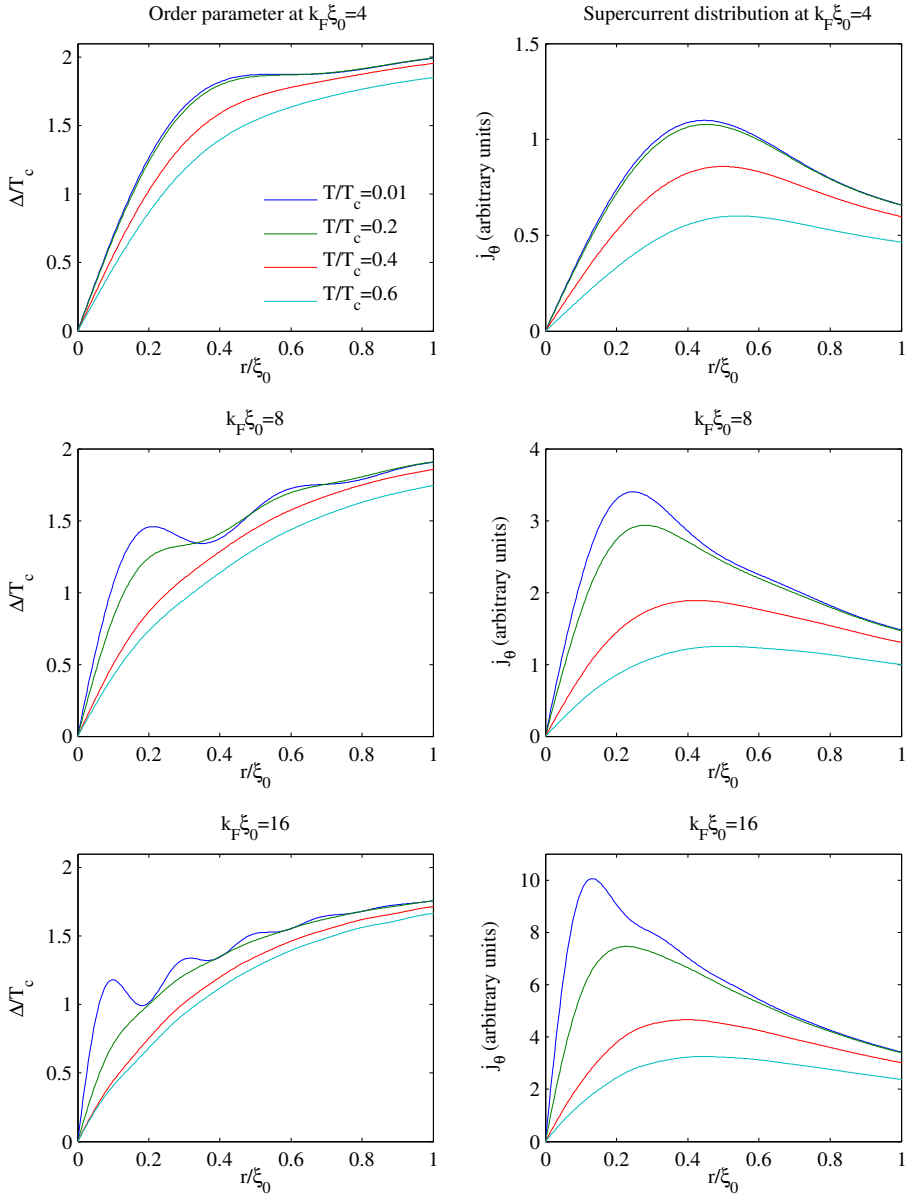

Figure 3.10: Order parameter and supercurrent profiles for different temperatures and different values of $k_F\xi_0$. As we approach the low temperature-limit, the order parameter – and to a lesser degree the supercurrent – exhibits oscillations. The wavelength of these increase as $k_F\xi_0$ decreases. We also see a saturation of the vortex core radius; it is larger for small $k_F\xi_0$, and becomes independent of temperature. These results are in good agreement with previous calculations by Hayashi et al. [29]; up to the choice of scale the plots for $k_F\xi_0 = 16$ are near-replications of figures 2–3 in their paper.

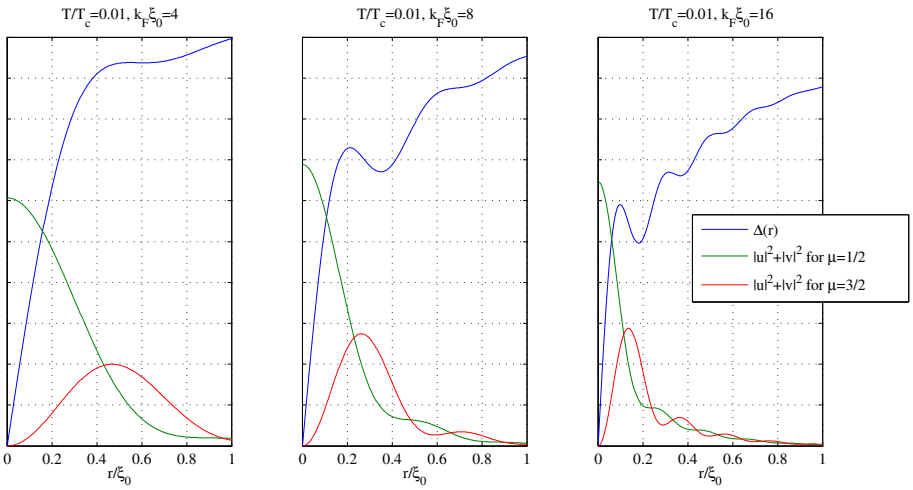

Figure 3.11: Order parameter profile together with the two lowest states.

is the appearance of oscillations in the order parameter at low temperature. The oscillations have a wavelength roughly proportional to $1/k_F\xi_0$, just like the lowest states. This supports the hypothesis that the source of the oscillations is the decreasing number of core states.

It is known that impurities in metals or semiconductors cause – at low temperatures – oscillations in the electron density of states. The reason for this is that the electron gas of the host material is rearranging to screen out the impurity charge. Since the temperature is low, the electrons of the gas all have energies in a narrow range around the Fermi surface and their wave functions have similar wave lengths. Only a few oscillatory modes thus contribute to the screening, and we see an oscillation in the density of states. This is known as Friedel oscillations [11]. We realize that the vortex core is an impurity in the otherwise homogeneous superconductor, so we can identify the oscillation in the order parameter as a Friedel oscillation in the quasiparticle density of states.

As for the supercurrent density, we are looking at the θ-component; the currents encircling the vortex line. The qualitative behaviour of this component – zero at the origin, rising to a peak and then decreasing as $1/r$ – is what we expect [8, 29]. The peak of the supercurrent becomes lower as $k_F\xi_0$ decreases; there are fewer states near the vortex core capable of carrying current. Friedel oscillations are present in the supercurrent profile as well, though they are more difficult to see. We find the reason for this in equation (3.38); the state $u_{j,\mu=1/2}$ – which is the dominant low-energy state – gives no contribution at all because of the factor $\mu - 1/2 = 0$. This is reasonable since $u_{j,\mu=1/2}(r)$ is symmetric around a peak at the core center and thus cannot carry angular momentum relative to the vortex; it follows that this state cannot cause any current that circulate the vortex core.

One way of thinking of superconductivity is that excitations from the ground state are created by breaking Cooper pairs [35], thus reducing the density of superconducting electrons. Since the order parameter is proportional to this density, we should be able to see a correlation between the minima in the order

parameter oscillation and the local density of states. Figure 3.11 is an indication that this is indeed the case. There, we have plotted the two lowest states together with the order parameter profile for $T/T_c = 0.01$. We see a very good correspondence between the vortex core radius and the width of the central peak of the $\mu = 1/2$-state. With a bit of good will, we can correlate the second minimum in $\Delta(r)$ with the peak in the $\mu = 3/2$-state, but the connection is tenacious at best. To solidify or reject this connection one would have to properly calculate the full spectral evolution of the system.

4 Summary and outlook

In this thesis, we have solved the Bogoliubov-de Gennes equations near a vortex line in an s-wave superconductor. We have investigated the low-temperature limit, and been able to well reproduce previously published results. From here, there are several directions of possible future work.

As mentioned in section 1, we hope to generalize the method to deal with d-wave and mixed parity superconductors. This involves a number of challenges. Perhaps the largest one is how to deal with an order parameter with angular dependencein an efficient way. In the case of superconductors with a p-wave component, how do we include the effects of spin?
Since the numerical complexity will increase, further optimization is required. One possible approach is to analytically study the matrix elements (3.21) in order to *a priori* determine which ones are significant, and minimize the number of performed numerical integrations.

Another approach is to remain in the s-wave superconductor and further investigate the low temperature-limit. Is there some way to determine if the found Friedel-like oscillation of the order parameter is just a numerical artefact? One possible path is by relaxing the restriction to a cylindrical Fermi surface, and keep the k_z^2-term in equation (3.6), and see if the oscillations remain. What happens at zero temperature? What happens if we do include a magnetic vector potential $\mathbf{A}$? How does the full density of states look? These are interesting questions, but perhaps not as relevant in the big picture as the first approach.

Bibliography

[1] J. G. Bednorz and K. A. Müller. Possible high T_c superconductivity in the Ba-La-Cu-O system. *Zeitschrift fur Physik B Condensed Matter*, 64:189–193, 1986.

[2] Victor J. Emery. The search for symmetry. *Nature*, 370:598, Aug 1994.

[3] C. C. Tsuei, J. R. Kirtley, C. C. Chi, Lock See Yu-Jahnes, A. Gupta, T. Shaw, J. Z. Sun, and M. B. Ketchen. Pairing symmetry and flux quantization in a tricrystal superconducting ring of $YBa_2Cu_3O_{7-\delta}$. *Phys. Rev. Lett.*, 73:593–596, Jul 1994.

[4] John R. Kirtley. Probing the order parameter symmetry in the cuprate high temperature superconductors by SQUID microscopy. *Comptes Rendus Physique*, 12(5–6):436 – 445, 2011.

[5] C. Caroli, P. G. de Gennes, and J. Matricon. Bound fermion states on a vortex line in a type II superconductor. *Physics Letters*, 9:307–309, May 1964.

[6] Øystein Fischer, Martin Kugler, Ivan Maggio-Aprile, Christophe Berthod, and Christoph Renner. Scanning tunneling spectroscopy of high-temperature superconductors. *Rev. Mod. Phys.*, 79:353–419, Mar 2007.

[7] Mikael Fogelström. Structure of the core of magnetic vortices in d-wave superconductors with a subdominant triplet pairing mechanism. *Phys. Rev. B*, 84:064530, Aug 2011.

[8] François Gygi and Michael Schlüter. Self-consistent electronic structure of a vortex line in a type-II superconductor. *Phys. Rev. B*, 43:7609–7621, Apr 1991.

[9] M. Franz and Z. Tešanović. Self-consistent electronic structure of a $d_{x^2-y^2}$ and a $d_{x^2-y^2} + id_{xy}$ vortex. *Phys. Rev. Lett.*, 80:4763–4766, May 1998.

[10] Michael Tinkham. *Introduction to Superconductivity*. McGraw-Hill, second edition, 1996.

[11] Neil Ashcroft and David Mermin. *Solid State Physics*. Brooks/Cole, first edition, 1976.

[12] H. Kamerlingh Onnes. Further experiments with liquid helium. D. On the change of electrical resistance of pure metals at very low temperatures, etc. V. The disappearance of the resistance of mercury. *Proceedings*, 14:113–115, 1911.

[13] J. Bardeen, L. N. Cooper, and J. R. Schrieffer. Theory of superconductivity. *Phys. Rev.*, 108:1175–1204, Dec 1957.

[14] Leon N. Cooper. Bound electron pairs in a degenerate fermi gas. *Phys. Rev.*, 104:1189–1190, Nov 1956.

[15] N. N. Bogoliubov, V. V. Tolmachev, and D. V. Shirkov. *A new method in the theory of Superconductivity.* Consultants Bureau, Inc., first edition, 1959.

[16] V. Ginzburg. On the theory of superconductivity. *Il Nuovo Cimento (1955-1965)*, 2:1234–1250, Dec 1955.

[17] Gor'kov L. P. Microscopic derivation of the Ginzburg-Landau equations in the theory of superconductivity. *Soviet Physics JETP*, 9:1364–1367, 1959.

[18] John S. Townsend. *A Modern Approach to Quantum Mechanics.* University Science Books, 2000.

[19] Barbara Goss Levi. In high-T_c superconductors, is d-wave the new wave? *Physics Today*, 46:17–20, May 1993.

[20] J. P. Carbotte. Coupling strength of charge carriers to spin fluctuations in high-temperature superconductors. *Nature*, 401(5624):354–356, Sep 1999.

[21] Charles Day. Iron-based superconductors. *Physics Today*, 62:36–40, Aug 2009.

[22] A.A. Abrikosov. On the magnetic properties of superconductors of the second group. *Soviet Physics JETP*, 5:1174–1182, Dec 1957.

[23] Pierre-Gilles de Gennes. *Superconductivity of Metals and Alloys.* Advanced Books Classics, reprint of first edition, 1989.

[24] Stephen Roman. *Advanced Linear Algebra.* Springer, second edition, 2005.

[25] John Bardeen, R. Kümmel, A. E. Jacobs, and L. Tewordt. Structure of vortex lines in pure superconductors. *Phys. Rev.*, 187:556–569, Nov 1969.

[26] Bascom S. Deaver and William M. Fairbank. Experimental evidence for quantized flux in superconducting cylinders. *Phys. Rev. Lett.*, 7:43–46, Jul 1961.

[27] R. Doll and M. Näbauer. Experimental proof of magnetic flux quantization in a superconducting ring. *Phys. Rev. Lett.*, 7:51–52, Jul 1961.

[28] John David Jackson. *Classical Electrodynamics.* John Wiley & Sons, third edition, 1999.

[29] N. Hayashi, T. Isoshima, M. Ichioka, and K. Machida. Low-lying quasiparticle excitations around a vortex core in quantum limit. *Phys. Rev. Lett.*, 80:2921–2924, Mar 1998.

[30] Michael R. Norman. Fermi-surface reconstruction and the origin of high-temperature superconductivity. *Physics*, 3:86, Oct 2010.

[31] Milton Abramowitz and Irene A. Stegun. *Handbook of Mathematical Functions with Formulas, Graphs, and Mathematical Tables.* U.S. Department of Commerce, tenth edition, 1972.

[32] H. F. Hess, R. B. Robinson, R. C. Dynes, J. M. Valles, and J. V. Waszczak. Scanning-tunneling-microscope observation of the Abrikosov flux lattice

and the density of states near and inside a fluxoid. *Phys. Rev. Lett.*, 62:214–216, Jan 1989.

[33] H. F. Hess, R. B. Robinson, and J. V. Waszczak. Vortex-core structure observed with a scanning tunneling microscope. *Phys. Rev. Lett.*, 64:2711–2714, May 1990.

[34] Hitoshi Nishimori, Kazuharu Uchiyama, Shin ichi Kaneko, Akio Tokura, Hiroyuki Takeya, Kazuto Hirata, and Nobuhiko Nishida. First observation of the fourfold-symmetric and quantum regime vortex core in YNi_2B_2C by scanning tunneling microscopy and spectroscopy. *Journal of the Physical Society of Japan*, 73(12):3247–3250, 2004.

[35] Bernhard Keimer. Broken cooper pairs caught bouncing around. *Science*, 300(5624):1381–1382, 2003.